Chemistry and Physics of Lipids 243 (2022) 105173

Contents lists available at ScienceDirect

Chemistry and Physics of Lipids

journal homepage: www.elsevier.com/locate/chemphyslip

Research paper

# What different physical techniques can disclose about disruptions on membrane structure caused by the antimicrobial peptide Hylin a1 and a more positively charged analogue

Gabriel S. Vignoli Muniz [a,*], Evandro L. Duarte [a], Esteban N. Lorenzón [b], Eduardo M. Cilli [c], M. Teresa Lamy [a,*]

[a] Instituto de Física, Universidade de São Paulo, Rua do Matão, 1371, 05508-090 São Paulo, SP, Brazil
[b] Unidade Acadêmica Especial Ciências da Saúde, Universidade Federal de Jataí, 75804-020 Jataí, GO, Brazil
[c] Instituto de Química, Universidade Estadual Paulista, Araraquara 14800-900, SP, Brazil

ARTICLE INFO

*Keywords:*
Antimicrobial peptide
Laurdan
Differential Scanning Calorimetry
Spin label
Liposomes
Carboxyfluorescein assay

ABSTRACT

The present work monitors structural changes in anionic membranes (DPPG; 1,2-dipalmitoyl-*sn*-glycero-3-phospho-(1′-*rac*-glycerol)) caused by the native antimicrobial peptide (AMP) Hylin a1 (Hya1; IFGAIL-PLALGALKNLIK-$NH_2$) and its synthetic analogue $K^0$Hya1 (**K**IFGAILPLALGALKNLIK-$NH_2$), with an extra positive residue of lysine at the N-terminus of the peptide chain. Anionic membranes were used to mimic anionic lipids in bacteria membranes. Differential scanning calorimetry (DSC) evinced that both peptides strongly disrupt the lipid bilayers. However, whereas the native peptide (+3) induces a space-average and/or time-average disruption on DPPG bilayers, the more charged, $K^0$Hya1 (+4), appears to be strongly attached to the membrane, clearly giving rise to the coexistence of two different lipid regions, one depleted of peptide and another one peptide-disrupted. The membrane fluorescent probe Laurdan indicates that, in average, the peptides increase the bilayer packing of fluid DPPG (above the lipid gel-fluid transition temperature) and/or decrease its polarity. Spin labels, incorporated into DPPG membrane, confirm, and extend the results obtained with Laurdan, indicating that the peptides increase the lipid packing both in gel and fluid DPPG bilayers. Therefore, our results confirm that Laurdan is often unable to monitor structural modifications induced on gel membranes by exogenous molecules. Through the measurement of the leakage of entrapped carboxyfluorescein (CF), a fluorescent dye, in DPPG large unilamellar vesicles it was possible to show that both peptides induce pore formation in DPPG bilayers. Furthermore, CF experiments show that Hylin peptides are strongly bound to DPPG bilayers in the gel phase, not being able to migrate to other DPPG vesicles. Here we discuss the complementarity of different techniques in monitoring structural alterations caused on lipid bilayers by Hylin peptides, and how it could be used to help in the understanding of the action of other exogenous molecules on biological membranes.

## 1. Introduction

Biological membranes are an extremely complex ensemble formed by asymmetric lipid bilayers composed of different phospholipids species, containing several molecules such as steroids, proteins, and carbohydrates (Alberts, 2008). The integrity of the membrane is preserved by inter molecular interactions among the membrane constituents and the interactions between the membrane and the surrounding aqueous molecules. Additionally, the cell's machinery maintains a precise control of membrane's physicochemical properties (Ohmann et al., 2018).

Given the complexity of biological membranes, simple mimetic systems, such as liposomes, are extremely useful to investigate the interaction of drugs with biological membranes and might reveal aspects about the drugs bioavailability, toxicity, and performance against pathogens (Seddon et al., 2009; Peetla et al., 2009). Accordingly, information about the changes induced in lipid's structure/dynamic by an exogenous agent has a pivotal relevance and may help the design of new therapeutic agents and to better comprehend their action.

Due to the emergence of new diseases, as well as the resistance of pathogens to traditional medications, the search for new therapeutic

* Corresponding authors.
*E-mail addresses:* gvignoli@if.usp.br (G.S. Vignoli Muniz), mtlamy@usp.br (M.T. Lamy).

https://doi.org/10.1016/j.chemphyslip.2022.105173
Received 5 October 2021; Received in revised form 15 December 2021; Accepted 2 January 2022
Available online 5 January 2022

agents has been a concern to the scientific community and a true challenge to contemporary science (Freedman, 2019; Rudrapal et al., 2020). Among the many molecules with potential therapeutic application, antimicrobial peptides (AMPs) have attracted attention (Wu et al., 2018; Pizzolato-Cezar et al., 2019; Datta and Roy, 2021).

AMPs are a group of amphiphilic molecules that usually display a positive net charge at physiological pH. They are present in virtually all living beings, with more than 3000 different AMPs already identified (Drider and Rebuffat, 2011; Wang et al., 2016). Some AMPs present a strong action against pathogens and parasites, affecting bacteria (Phoenix et al., 2013), protozoa (Rivas et al., 2009) and even displaying antiviral (Chessa et al., 2020) and antitumoral (Tornesello et al., 2020) activities. AMPs can be designed, aiming at the increase of their action against pathogens/tumors and the reduction of their toxic effects against healthy cells (Reinhardt and Neundorf, 2016). The AMPs exact mechanisms of action are still a matter of discussion (Brogden, 2005; Raheem and Straus, 2019). However, given their amphipathic character, many AMPs strongly interact with lipid bilayers. Particularly, it has been proposed that cationic AMPs would preferentially interact with anionic lipids present on the outer bacterial membrane (Phoenix et al., 2013; Sani and Separovic, 2016; (Mingeot-Leclercq and Décout, 2016).

Hylin a1 (IFGAILPLALGALKNLIK-$NH_2$) is an AMP extracted from the skin secretion of the frog *Hypsiboas albopunctatus*, native from South America (Castro et al., 2009). *In vitro*, Hylin a1 (Hya1) presents a strong action against bacteria and fungus, but considerable hemolytic action also (Castro et al., 2009; Crusca et al., 2011). Peptides from the Hylin a1 family have been shown to strongly interact with model membranes, and the peptide net charge was found to play a key role in their interaction with lipid bilayers (Alves et al., 2015; Enoki et al., 2018; Santana et al., 2020; (Vignoli Muniz et al., 2020).

In the present work, we comparatively investigate the interaction of the native peptide Hya1 and its more positively charged analogue $K^0$Hya1 (**K**IFGAILPLALGALKNLIK-$NH_2$), (Fig. 1), with a simple model of bacterial membrane, namely anionic liposomes composed of 1,2-dipalmitoyl-*sn*-glycero-3-phospho-(1′-*rac*-glycerol) (DPPG), as PG is the most abundant anionic headgroup in bacterial membrane lipids (Marsh, 2013; Mingeot-Leclercq and Décout, 2016). DPPG membranes present a gel-fluid transition temperature at approximately 40 ºC (Heimburg, 2007). Hence, varying the temperature from 15 ºC to 60 ºC, it was possible to investigate the action of Hya1 and $K^0$Hya1 on gel and fluid DPPG bilayers, mimicking both more and less packed lipid domains in bacterial membranes.

Using the two peptides, Hya1 and $K^0$Hya1, and anionic vesicles, we focus on the effect of the extra electric charge on the interaction of the peptides with lipid bilayers. Moreover, the electrostatic attraction between peptides and lipid membranes was enhanced by using low ionic strength medium and pure PG bilayers, therefore increasing the concentration of peptide around the vesicles.

Different methodologies were applied. With differential scanning calorimetry (DSC) it was possible to monitor the changes caused by the peptides on the gel-fluid transition of the DPPG membrane. The structure and dynamics of the nanoregion close to the DPPG surface were monitored by steady-state and time-resolved fluorescence spectroscopy using the fluorescent probe 2–dimethylamino-(6–lauroyl)-naphthalene (Laurdan), and electron spin resonance (ESR) using the paramagnetic probe 1-palmitoyl-2-(5-doxylstearoyl)-sn-glycero-3-phosphocholine (5-PCSL), both probes incorporated into DPPG bilayers. Furthermore, through the measurement of the leakage of entrapped carboxyfluorescein (CF), a fluorescent dye, in DPPG large unilamellar vesicles (LUVs), we quantified the ability of the Hylin peptides to induce pore formation in DPPG vesicles and their ability to migrate among different DPPG vesicles. Hence, this work discusses how different experimental approaches are necessary for a comprehensive understanding of the structural effects caused on a lipid membrane by two similar peptides which differ only by a lysine residue.

**Hya1** (+3)

$NH_3^+$ IFGAILPLALGALK$^+$NLIK$^+$$NH_2$

**$K^0$Hya1** (+4)

$NH_3^+$**K**$^+$IFGAILPLALGALK$^+$NLIK$^+$$NH_2$

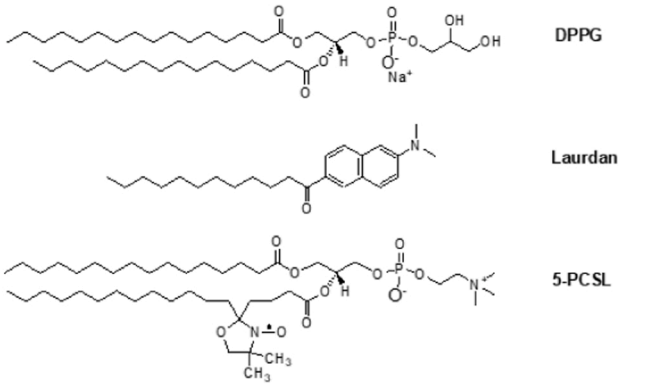


**Fig. 1.** From top to bottom: primary structures of the AMPs Hya1 and $K^0$Hya1, and the chemical structures of the lipid DPPG, the fluorescent probe Laurdan, and the spin probe 5-PCSL. Polar amino acid residues are indicated in blue and non-polar in red. The net charges of the peptides are indicated in parentheses. The inserted lysine residue in $K^0$Hya1 is indicated in bold. (For interpretation of the references to colour in this figure legend, the reader is referred to the web version of this article.)

## 2. Material & methods

### 2.1. Materials

2–dimethylamino-(6–lauroyl)-naphthalene (Laurdan) probe was purchased from Molecular Probes Inc. (Eugene, OR, USA). Sodium salt of 1,2-dipalmitoyl-sn-glycero-3-phospho-(1′-rac-glycerol) (DPPG), sodium salt of 1-palmitoyl-2-oleoyl-sn-glycero-3-phospho-(1′-rac-glycerol) (POPG), cholesterol, and spin label 5-PCSL were purchased from Avanti Polar Lipids (Alabaster, AL). 4-(2-hydroxyethyl)− 1-piperazineethanesulfonic acid (HEPES), ethylenediaminetetraacetic acid (EDTA), Triton X-100, chloroform, methanol, NaCl, Sephadex-G25 columns, 5(6)-Carboxyfluorescein (CF), glucose, ammonium molybdate, citric acid, perchloric acid, sodium hydroxide (NaOH), and hydrochloric acid (HCL) were purchased from Merck (St. Louis, MO).

### 2.2. Peptide synthesis

The peptides were synthesized manually using the Fmoc strategy, purified, and characterized according to the experimental protocol described in details elsewhere (Crusca et al., 2011). The purity of Hylin peptides was found to be higher than 97.8%. Hya1 and $K^0$Hya1 molecular weight were determined as 1992.5 g $mol^{-1}$ and 1864.1 g $mol^{-1}$, respectively, by mass spectrometry (Fig. SM1 and SM2).

### 2.3. Large unilamellar vesicles (LUVs) preparations

Lipids were dissolved in a mixture of chloroform and methanol (6:1). When desired, Laurdan (1 mol%) or spin label 5-PCSL (0.8 mol%), relative to the lipid concentration, were added to the lipid solution. The

lipid solution was dried under a stream of ultra-pure nitrogen gas till a thin film of lipids was formed at the bottom of the glass tube. Then, the lipid film was kept under low pressure conditions for a minimum of three hours to eliminate any trace of organic solvents. Lipid dispersions were prepared by the addition of buffer (10 mmol $L^{-1}$ HEPES, 3 mmol $L^{-1}$ NaCl, 1 mmol $L^{-1}$ EDTA, pH 7.4) to the lipid film, followed by intense vortexing during 2 min at 60 °C, four times. Finally, lipid dispersions were extruded through polycarbonate filters (mini-extruder by Avanti Polar Lipids, 19 mm membranes with 100 nm pores, 31 times) above the lipid gel−fluid transition temperature (≥ 60 °C), for the formation of large unilamellar vesicles (LUVs). After extrusion, the average diameter of the vesicles was verified using dynamic light scattering and found to be (110 ± 10) nm. Before and after filtering, a few DPPG samples were checked for their phospholipid content through inorganic phosphate assay (Rouser et al., 1966), and the error was always found to be less than 1% of the expected value for samples before filtering, and less than 3% after the filtering process. All lipid dispersions used in this work were freshly prepared on the day the experiment was conducted. They were prepared at the concentration to be used in each experiment, as stated bellow, considering the necessary dilution due to the addition of the peptide solution.

### 2.4. Differential scanning calorimetry (DSC)

Calorimetric measurements were performed using a microcalorimeter (Microcal VP-DSC, Northampton, MA). Each sample was scanned five times. The first scan was performed at 90 °C per hour, and discarded. The next four scans, two endothermic and two exothermic, were run at the rate of 20 °C per hour, with temperatures ranging from 15 °C to 60 °C. The scans were found to be fairly reproductible. The sample cell (500 μL) was filled with a 3 mmol $L^{-1}$ lipid dispersion with and without the desired AMP concentration. In this work, we often refer to the concentration of AMP as the percentage of the peptide with respect to the molar concentration of the lipid (mol% [AMP] = 100 [AMP]/[DPPG]), where [AMP] and [DPPG] are AMP and DPPG molar concentrations, respectively. By using MicroCal Origin software, with the additional module for DSC data analysis provided by MicroCal, we determined thermodynamic parameters such as the excess enthalpy ($\Delta H$), the position of the maximum of the gel-fluid temperature transition peak, $T_m$, and the width at half maximum ($\Delta T_{1/2}$).

### 2.5. Ultraviolet-visible (UV–vis) absorption measurements

Optical absorption spectra were obtained with an UV−vis spectrophotometer (Varian Cary 50, Santa Clara, CA). In all optical experiments, samples were placed in a quartz cuvette (0.2 × 1.0 cm, 400 μL), with the absorption optical pathway of 0.2 cm. The temperature was controlled with a Carry Peltier thermostat.

500 μmol $L^{-1}$ extruded DPPG dispersion labeled with Laurdan (5 μmol $L^{-1}$), with and without a given AMP concentration, was used. The samples were incubated at room temperature for at least 30 min just prior to the experiments. Then, the sample was placed in the spectrometer preset at 15 °C. To assure the thermal equilibrium, the sample was left for 15 min inside the spectrometer. The optical experiments were conducted in sequence: first the absorption spectrum was registered, then the steady-state fluorescence spectrum, finally the fluorescence decay was measured. At the end of each sequence of measurements the temperature was increased, and the same protocol was followed. The optical experiments using Laurdan were performed with temperatures ranging from 15 °C to 60 °C.

### 2.6. Steady-State fluorescence measurements

Steady-state fluorescence measurements were performed with a fluorimeter (Varian Eclipse, Santa Clara, CA) with temperatures controlled by a Carry Peltier thermostat. The samples consist of 500 μmol $L^{-1}$ extruded DPPG dispersion labeled with Laurdan (5 μmol $L^{-1}$) with and without a given AMP concentration. The experiments were conducted with an excitation beam light at 340 nm, with an optical pathway for excitation of 0.2 cm, quartz cuvette (0.2 × 1.0 cm, 400 μL), with slits for excitation and for emission of 5 nm. The inner filter correction (Lakowicz, 2006) was applied to all the fluorescent emission spectra by using the Eq. 1:

$$F_{corr}(\lambda) = F_{obs}(\lambda)10^{(A_{exc} \quad l+A_{ems}(\lambda)l')} \tag{1}$$

where $F_{corr}$ (λ) and $F_{obs}$ (λ) are the corrected and observed fluorescence intensities, $A_{exc}$ and $A_{ems}$ (λ) are the absorbance per unit of pathway at the excitation and emission wavelengths, respectively. l and l′ are the optical pathway in cm for excitation (0.1 cm), and for emission (0.5 cm), respectively, considering the cuvette center. Note that Eq. 1 does not consider the dimensions of the excited region, as it is assumed that all emitting fluorophores are at the center of the cuvette. It has been shown that this equation is suitable for the absorbance values used here (Mendonça et al. 2013).

After the corrections, to transform Laurdan spectra from wavelength (λ) to energy, the emission spectra were multiplied by $\lambda^2$. This procedure is necessary given that the fluorescence spectra were recorded with a constant bandpass wavelength (Valeur, 2002; Vequi-Suplicy et al., 2015).

In this work, Laurdan spectra in energy were decomposed into Gaussians. It was not possible to fit Laurdan emission with only one Gaussian band with a reduced chi-square close to the unity. Therefore, it was necessary to fit the Laurdan spectra with at least two Gaussian bands, see Fig. SM3.

### 2.7. Time-Resolved fluorescence measurements

Time-resolved (TR) fluorescence measurements were performed using the time-correlated single photon counting technique (TCSPC). The excitation light beam comes from a titanium-sapphire Tsunami 3950 laser from Spectra Physics (Newport Corporation, Irvine, CA, USA), pumped by a solid-state laser Millenia Pro model J80 also from Spectra Physics. The frequency of the pulse picker (Spectra Physics model 3980–25) was 8 MHz. The Tsunami was set to give an output of 852 nm and a third harmonic generator BBO crystal (GWN-23PL Spectra Physics) was used to generate the excitation light at 284 nm. Although this is different from the excitation wavelength used in the steady state fluorescence, 340 nm, it also corresponds to an absorption band of Laurdan, and Laurdan fluorescence relaxation was shown not to depend on the excitation wavelength (Masukawa et al., 2019). At 284 nm, the signal-to-noise was found to be much better than at 340 nm. The emission was detected at 90 degrees from the excitation beam and selected by a monochromator.

By using FAST software supplied by Edinburgh Photonics the data were fitted by applying the model of exponential decays (Lakowicz, 2006) using the following equations:

$$F(\lambda, t) = \sum_{i=1}^{N} \alpha_i e^{-t/\tau_i} \tag{2}$$

$$f_i = \frac{\alpha_i \tau_i}{\sum_j \alpha_j \tau_j}$$

where F(λ,t) is the number of photons emitted at a given wavelength (λ) and time (t), $\alpha_i$ is the pre-exponential factor, $\tau_i$ is the lifetime of the $i^{th}$ component of the decay, and $f_i$ is the fraction contribution of the lifetime $\tau_i$ to the intensity decay. The values were determined from the best fitting processes which resulted from the statistical parameter reduced chi-square ($\chi^2$), $0.95 \leq \chi^2 \leq 1.35$.

### 2.8. Electron spin resonance (ESR) spectroscopy

X-band (9.44 GHz) electron paramagnetic resonance spectra were obtained with a Bruker EMX spectrometer. Field-modulation of 1 or 2G and microwave power of 5 mW were used. The temperature ranged from 15 ºC to 60 ºC, controlled by a Bruker BVT-2000 variable temperature device. ESR data were analyzed using the software WINEPR. The maximum ($2A_{max}$), and minimum ($2A_{min}$) hyperfine splittings were measured directly on the ESR spectrum, see Fig. 8. For fluid membranes, the effective order parameter ($S_{eff}$) and the isotropic hyperfine splitting ($a_0$) were calculated according to the equations (Rozenfeld et al., 2017):

$$S_{eff} = \frac{A_{\parallel} - A_{\perp}}{A_{zz} - (1/2)(A_{xx} + A_{yy})} \frac{a_o^{'}}{a_o} \quad (3)$$

$$where \quad A_{\parallel} \approx A_{max}$$

$$A_{\perp} = A_{min} + 1.4 \left[1 - \frac{A_{\parallel} - A_{min}}{A_{zz} - \left(\frac{1}{2}\right)(A_{xx} + A_{yy})}\right]$$

$$a_0^{'} = 1/3(A_{zz} + A_{yy} + A_{xx})$$

$$a_0 = 1/3(A_{\parallel} + 2A_{\perp})$$

The lipid concentration used was 3 mmol $L^{-1}$, with and without the desired peptide concentration.

### 2.9. Entrapment of carboxyfluorescein (CF) in LUVs: Leakage assay

CF solutions were prepared in buffer pH 8.5. After CF solubilization, the sample pH was readjusted to 7.4 with HCl. Lipid films were hydrated with buffer solution (10 mmol $L^{-1}$ HEPES, 3 mmol $L^{-1}$ NaCl, 1 mmol $L^{-1}$ EDTA, pH 7.4) containing 50 mmol $L^{-1}$ carboxyfluorescein (CF). The lipid dispersion (~6 mmol $L^{-1}$) was extruded, as previously described. In order to remove non-encapsulated CF, the lipid dispersion was eluted through a Sephadex-G25 medium column with 10 mmol $L^{-1}$ HEPES, pH 7.4 with 1 mmol $L^{-1}$ EDTA, 3 mmol $L^{-1}$ NaCl, and 150 mmol $L^{-1}$ glucose, the latter was added to the buffer to adjust the osmolarity inside and outside the liposomes. Vesicles with encapsulated CF were collected in the void volume of the column. Lipid concentration was determined by inorganic phosphate assay (Rouser et al., 1966).

CF encapsulated in LUVs was used to evaluate the ability of Hylin peptides to induce pore formation in the PG bilayers. At 50 mmol $L^{-1}$ the encapsulated CF is self-quenched, hence almost non-fluorescent. Due to AMPs or detergent action, CF might be released into the aqueous bulk, where dilution occurs, thus yielding an increase of CF fluorescence intensity. CF emission was continuously recorded in time (one measurement per second), at 25 °C, $\lambda_{exc}$ = 490 nm and $\lambda_{em}$ = 512 nm.

Two different experiments were performed. At the first, LUVs (100 μmol $L^{-1}$) containing CF were placed in quartz cuvettes (1.0 × 1.0 cm, 2.0 mL) and the fluorescent emission measured with a Fluorescence Spectrometer (Varian Cary Eclipse, Santa Clara, CA), with temperatures controlled by a Carry Peltier thermostat, 25 ºC. The CF leakage measurements were performed under constant stirring. At the 100th second, the AMPs (8 μmol $L^{-1}$) were injected in the sample, and at the end of the experiment, at the 2000th second, Triton X-100 (18 μL of 10% w/v) was injected into the lipid dispersion to promote complete CF leakage.

The second experiment consisted of monitoring 100 μmol $L^{-1}$ DPPG dispersions with AMPs (8 μmol $L^{-1}$) placed in quartz cuvettes (1.0 ×1.0 cm, 2.0 mL) in the fluorimeter pre-set at 25 ºC, under constant stirring for 33 min. Then, at the 100th second, we added to the cuvette a DPPG dispersion containing CF inside the vesicles (100 μmol $L^{-1}$, 2 mL). At end of the experiments, at the 2000th second, Triton X-100 (18 μL of 10% w/v) was injected into the quartz cuvette to promote complete CF leakage.

For both experiments, the percentage of CF leakage, (%) Leakage, was determined according to the following equation:

$$(\%)Leakage \quad (t) = \quad 100 \quad \times \quad (I(t) - \quad I_0)/(I_{Total} - I_0) \quad (4)$$

where I(t) is the fluorescence intensity at time t, $I_0$ is the initial fluorescence, before the AMP addition, or in the second experiment $I_0$ is the fluorescence intensity registered 30 s after the addition of LUVs containing CF. $I_{Total}$ is the maximum fluorescence obtained after the addition of Triton X-100. As the experimental procedure with fluid DPPG (50 °C) was found to be quite unreliable (Vignoli Muniz et al., 2020), to mimic the fluid phase of the dipalmitoyl membranes similarly prepared vesicles of POPG were used at 25ºC.

For a clearer understanding of the leakage processes, the kinetics profiles were analyzed considering exponential processes (Almeida and Pokorny, 2010). Hence, the decay curves were fit with the minimum number of terms displayed in the equation below

$$\%\ Leakage\ (t) = A_1\left(1 - e^{-t/T_1}\right) + A_2\left(1 - e^{-t/T_2}\right) + A_3\left(1 - e^{-t/T_3}\right) + ( \quad (5)$$

Here, CF leakage kinetics could be characterized by two different processes only, with different decay times: $T_1$ and $T_2$, with $T_1 < T_2$. $A_1$ and $A_2$ are the percentages of CF leakage at the end of the processes 1 and 2, which decay with their characteristic times. The total percentage of leakage induced by the peptides is given by $A_T = A_1 + A_2$.

### 2.10. Reproducibility and sample stability

Every experiment was performed at least two times. Error values account for standard deviations and are presented as error bars when larger than the symbols.

No vesicle precipitation was observed during the experiments. The samples were always visually checked before and after the measurements were taken. For optical absorption and fluorescence measurements, Laurdan spectra were quite reproducible after at least 3 h.

## 3. Results & discussions

### 3.1. Differential scanning calorimetry (DSC)

Liposomes composed of only one species of saturated lipids often exhibit a very narrow excess heat peak, determining the transition between two different thermal phases: a gel and a fluid phase (see, for instance, Heimburg, 2007). In both phases, the lipid molecules are confined in the two-dimensional plane of the bilayer. However, in the gel phase, the lipids are more packed, with a higher restriction of mobility and display a lateral order, whereas in the fluid phase the lipids are wobbling along the axis of the bilayer in a more isotropic motion in comparison with the lipids in the gel phase (Heimburg, 2007).

Multilamellar dispersions frequently display a pretransition peak, which is a less pronounced thermal peak that occurs at temperatures lower than that of the main transition peak ($T_m$). Extruded (through 100 nm filter) dipalmitoyl dispersions display a very smooth and subtle pretransition peak. Moreover, the gel-fluid transition of extruded DPPG vesicles is less cooperative (larger width at half maximum, $\Delta T_{1/2}$) than that found for DPPG multilamellar vesicles (Enoki et al., 2012). These effects have been attributed to changes in the liposome curvature (Heimburg, 2007).

Lipid melting is very dependent on lipid-lipid interaction, and might be profoundly perturbed by an exogenous molecule, hence DSC is a suitable technique to investigate the interaction between a molecule and lipid bilayers (Prenner and Chiu, 2011).

Peptide solutions used here, up to 300 μmol $L^{-1}$, do not display any excess heat peak (Fig. SM4), this is a strong indication that the peptides are unstructured in solution, as observed for some Hylin a1 analogues

(Crusca et al., 2017). Therefore, DSC thermograms shown here are only monitoring DPPG membranes, and the changes induced on them by the peptides. Fig. 2 shows typical thermograms of extruded 3 mmol $L^{-1}$ DPPG dispersions in the absence and in the presence of increasing concentrations of the native peptide Hya1 (Fig. 2a) and its analogue, $K^0$Hya1, (Fig. 2b). The thermodynamic parameters of extruded DPPG dispersion are in good accordance with data in the literature (Riske et al., 2009; Enoki et al., 2018; Vignoli Muniz et al., 2021), with $T_m$ = (39.5 ± 0.3) ºC, $\Delta H$ (enthalpy variation) = (8.7 ± 0.3) kcal $mol^{-1}$ and $\Delta T_{1/2}$ = (0.67 ± 0.02) ºC.

At the peptide/lipid molar concentrations used here, Fig. 2 shows that the two peptides drastically change the DPPG thermal profile, indicating that both peptides interact with DPPG membranes.

However, the changes caused on the DPPG thermal profile by the two peptides are quite different. The effect of $K^0$Hya1 on the DPPG membrane is similar to that detected with the analogue $K^0$-$W^6$-Hya1, which has the same electric charge as $K^0$Hya1 (+4), but where a Leu was replaced by the fluorescent and more hydrophobic residue Trp at the 6th position (Enoki et al., 2018). Namely, as the [P]/[L] molar ratio increases, a new thermal event grows up at a lower temperature (36.04 ± 0.05) ºC, and coexists with an approximately pure lipid gel-fluid transition peak (39.5 ± 0.3) ºC, which decreases as the peptide concentration increases, clearly indicating the coexistence of peptide-bound and peptide-free regions in the bilayer. Note that at 6 mol %, only a small fraction of the pure DPPG thermal transition peak is observed (Fig. 2b) and at 10 mol% of $K^0$Hya1 just the peptide-lipid bound peak can be detected in Fig. 2b, indicating that there is no more bulk lipid membrane.

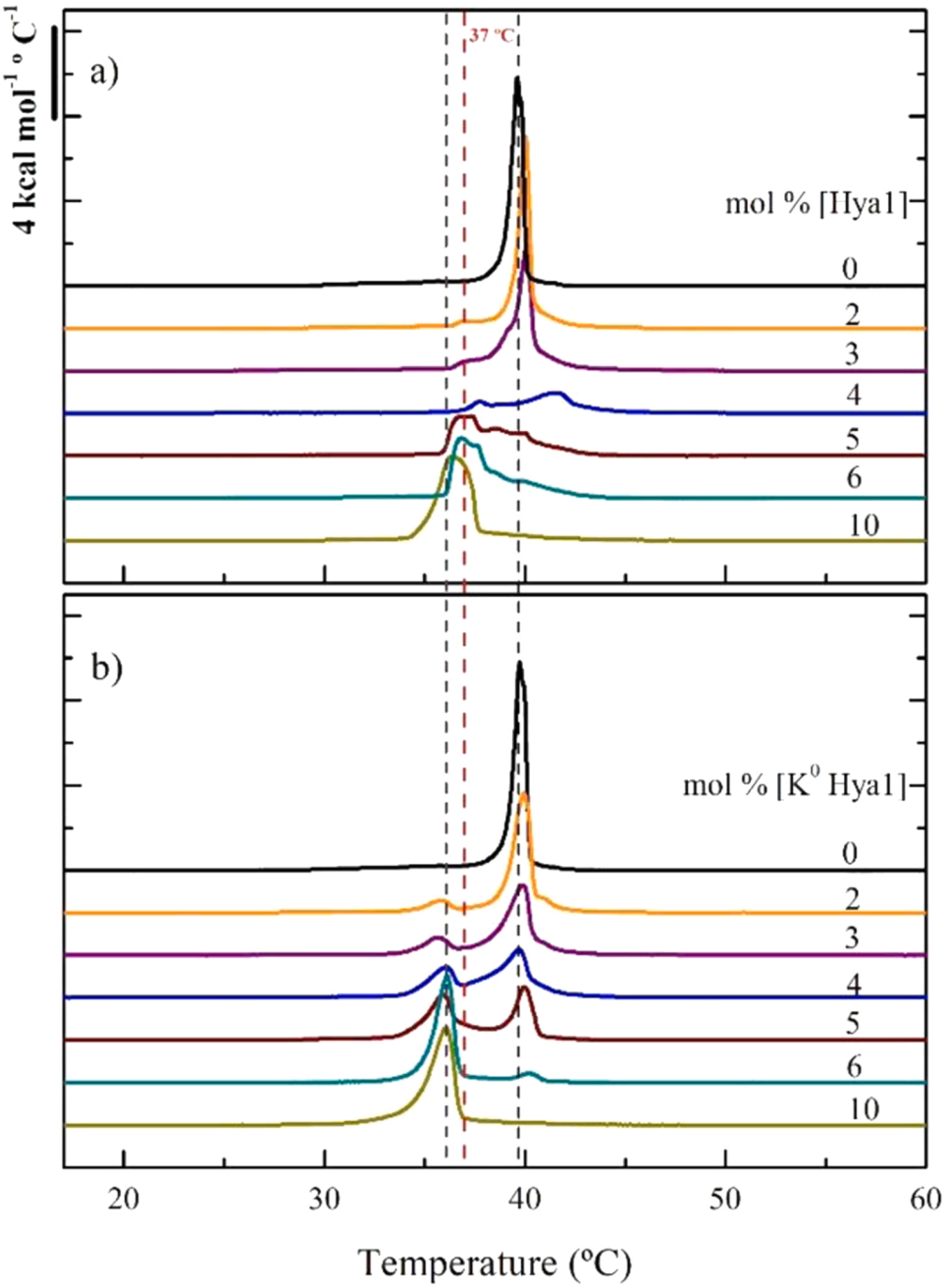


**Fig. 2.** DSC thermograms of extruded lipid dispersions composed of 3 mmol $L^{-1}$ DPPG with increasing peptide−lipid molar ratio, from 2% to 10% of (a) Hya1 or (b) $K^0$Hya1. Thermograms were obtained using a scan rate of + 20 °C/h, and they are shifted in the y-axis for clarity. Duplicated samples showed similar results. Dashed lines are guides for the eyes only. (For interpretation of the references to colour in this figure, the reader is referred to the web version of this article.)

On the other hand, with Hya1 (+3) (Fig. 2a), the presence of two thermal events is not well-defined, hence there is no clear coexistence of peptide-bound and peptide-free regions in the bilayer. This strongly suggests that the presence of the extra positively charged lysine residue, $K^0$, is crucial to peptide strong attachment to PG groups, giving rise to the coexistence of two different regions on the membrane. This effect is typical of a strong ionic interaction between a cationic molecule and anionic headgroups on the bilayer (Zweytick et al., 2014; (Pabst et al., 2008); Enoki et al., 2018; Vignoli Muniz et al., 2021).

For both peptides at 10 mol% relative to the lipid, DPPG undergoes a one peak gel-fluid transition, broader and at a lower temperature than that yielded by pure DPPG, indicating that the peptides penetrate into the bilayer and disrupt the liposome structure. Interestingly, in the presence of 10 mol% of the native peptide, Hya1, the gel-fluid DPPG transition peak is somehow broader, hence less cooperative, than that observed at the same concentration for the more cationic analogue, $K^0$Hya1.

For 4 and 6 mol% of $K^0$Hya1, a clear coexistence of bulk lipids and peptide-bound lipid domains is also observed at the temperature down-scan (Fig. 3d and f). As observed before with $K^0$-$W^6$-Hya1 (Enoki et al., 2018), bulk lipids display a rather reversible transition, but peptide-lipid domains display a significant hysteresis. The hysteresis is not so clear for the less charged peptide, Hya1, at 4 and 6 mol% (Fig. 3c and e). However, at 10 mol% peptide (Fig. 3g and h), the DSC up and down scans of both peptides display a significant thermal hysteresis. This is strong evidence of the penetration of the peptides into the gel and fluid phases of the DPPG membrane. Accordingly, these peptide-disrupted lipids in the fluid phase need a lower temperature to get more organized in a gel phase.

Interestingly, at 6 mol% of $K^0$Hya1 (Fig. 3f) the one up-scan thermal peak related to peptide-lipid domains turns into two peaks in the cooling process. These two peaks are still present at 10 mol% of the peptide (Fig. 3h), but the balance between them is altered. The spread of membrane gel-fluid transition into two or more peaks has been attributed to complex thermal processes (Lamy-Freund and Riske, 2003) and is out of the scope of the present work. The thermal processes undergone by DPPG in the presence of the peptides are quite reproducible, as illustrate for DPPG + 10 mol% $K^0$Hya1 in Fig. SM5.

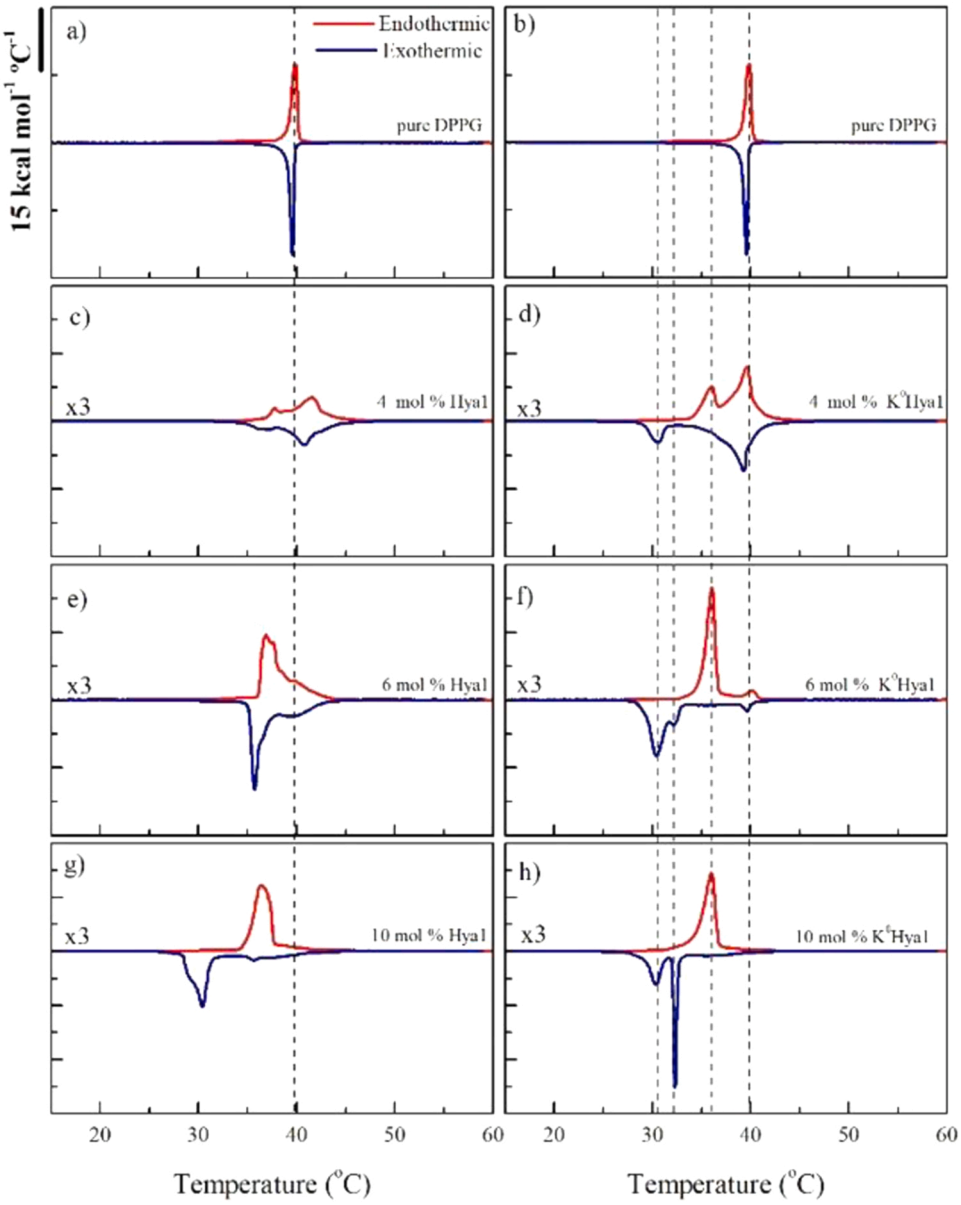


**Fig. 3.** Comparison of DSC thermograms of 3 mmol $L^{-1}$ DPPG under endothermic (red lines) and exothermic (blue lines) processes, in the absence (a,b), and in the presence of Hya1 (left column) and $K^0$Hya1 (right column), at different peptide/lipid concentrations: 4 mol% (c,d), 6 mol% (e,f), and 10 mol% (g,h). Dashed lines are guides for eyes only. DSC thermograms in the presence of the AMPs were amplified (indicated at the left of the traces) for better visualization. (For interpretation of the references to colour in this figure legend, the reader is referred to the web version of this article.)

### 3.2. Fluorescence spectroscopy: Laurdan as an extrinsic fluorescent probe

#### 3.2.1. Steady-state fluorescence

Extrinsic fluorescent probes are extremely useful to monitor structure/dynamics of model membranes and membranes of living cells (Valeur, 2002; Niko et al., 2016). For its versatility and low-cost, steady-state fluorescence spectroscopy has been a wide used technique to monitor the interaction between membranes and exogenous molecules. The probe Laurdan has been largely applied to investigate changes induced by drugs on liposomes, as its acyl tail ensures that this probe stays into the lipid bilayer, not partitioning in the aqueous environment (Weber and Farris, 1979). It has been proposed that the fluorescent moiety of Laurdan resides close to the interface between the acyl chain and the polar headgroups of the lipid bilayers (Parasassi et al., 1998; De Vequi-Suplicy et al., 2006). Hence, Laurdan probes the vicinity of the membrane surface. Due to its high excitation dipole, Laurdan is extremely sensitive to its environment's polarity and packing (Weber and Farris, 1979). Within lipid bilayers, Laurdan emission displays a significant red shift (~ 50 nm) when phospholipid membranes goes from the gel to the fluid phase (Parasassi et al., 1991). Laurdan fluorescence spectrum in different solvents, as well as within lipid bilayers, seems to be composed of two emission bands (Bacalum et al., 2013; Vequi-Suplicy et al., 2015). This dual emission has been attributed to a solvent-relaxed and a solvent-non-relaxed state (Parasassi et al., 1991, 1998). However, more recently, a new interpretation has been proposed, attributing the two bands to dual decays from independent singlet excited states (Vequi-Suplicy et al., 2015, 2020).

Laurdan generalized polarization (GP) is a commonly used parameter to monitor the fluidity/polarity of phospholipid bilayers. However, it has been shown that since GP is determined by using the fluorescence emission at two different wavelengths only, typically the intensities at 440 nm and 490 nm, a considerable amount of information is lost. For instance, GP could not detect the anomalous thermal transition of 1,2-dimyristoyl-sn-glycero-3-phospho-(1′-rac-glycerol) (DMPG) membranes at low ionic strength, well monitored by the decomposition of Laurdan fluorescence spectrum (Lúcio et al., 2010). Moreover, the spectrum decomposition allows the study of the positions of the emission bands and their areas, hence informing about the energies of the electronic transitions and the population of molecules relaxing from each excited state (see, for instance, Vequi-Suplicy et al., 2015; Masukawa et al., 2019). It is noteworthy to mention that, to be theoretically meaningful, the decomposition of the Laurdan spectrum in Gaussian bands must be

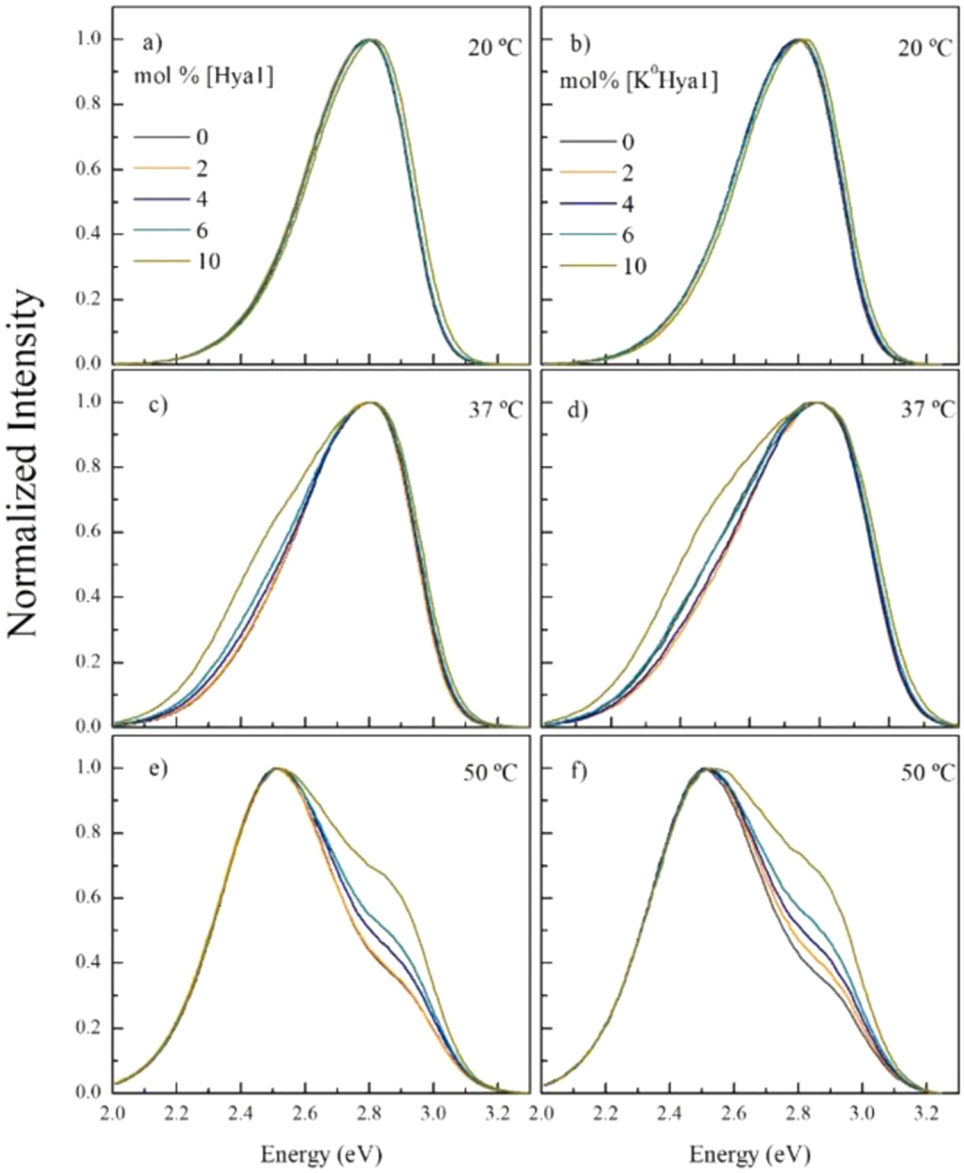


**Fig. 4.** Emission spectra of Laurdan (5 μmol $L^{-1}$) incorporated into DPPG (500 μmol $L^{-1}$) vesicles in the absence and with different concentrations of Hya1 (left column) or $K^0$Hya1 (right column), at three temperatures, 20 °C (a,b), 37 °C (c,d), and 50 °C (e,f). Peptide/lipid concentrations: 0 (black lines), 2 mol% (orange lines), 4 mol% (blue lines), 6 mol% (dark cyan lines), and 10 mol% (dark yellow lines). (For interpretation of the references to colour in this figure legend, the reader is referred to the web version of this article.)

performed in energy/wavenumber (see, for instance, Bransden and Joachain, 1986).

Let us examine the emission of Laurdan embedded into DPPG vesicles at different temperatures, with different amounts of peptide. In Fig. 4, the black lines correspond to Laurdan emission in the absence of peptides at three temperatures, at 20 ºC and 50 ºC, for all samples corresponding to the membranes in the gel and fluid phases, respectively, and at 37 ºC, temperature at which some samples with peptide have already undergone the gel-fluid transition (see DSC scans in Fig. 2). As expected, Laurdan fluorescence spectrum (Fig. 4, black lines) was found to be very sensitive to changes on the DPPG structure and/or membrane hydration due to the gel-fluid phase transition, (Parasassi et al., 1991). However, increasing amounts of both peptides do not change much the Laurdan spectrum at 20 ºC, at the DPPG gel phase (Fig. 4a and b). It is important to have in mind that Laurdan fluorescence spectrum could not detect changes caused by other exogenous membrane-interacting molecules that were found to alter the structure of the gel phase of lipid membranes, namely the melanotropic peptides α-MSH and NDP-α-MSH, and cholesterol (Lúcio et al., 2010, see also Fig. SM6). Additionally, it was shown that Laurdan could not detect significant structural differences in gel membranes composed of different lipids (Takechi-Haraya et al., 2018). Hence, interestingly, Laurdan fluorescence seems to be non-sensitive to changes on the structure of gel phase membranes.

Opposite to that, Laurdan emission in fluid DPPG vesicles, at 50 ºC (Fig. 4e and f), is significantly altered by the presence of the peptides. Increasing amounts of the peptides lead to deformation on the Laurdan emission spectra. Note that there is a clear increase of the probe's emission at higher energy. Interesting to note that Laurdan emission in fluid DPPG (Fig. SM6), or fluid DMPG, is severely altered by high cholesterol contents (Lúcio et al. 2010), also with a significant increase in the emission at high energies. Since it is largely known that cholesterol rigidifies and dehydrates fluid lipid bilayers (Marsh, 1981), it seems that the changes on the Laurdan emission profile are related to the packing and/or the dehydration caused by Hya1 and its more positively

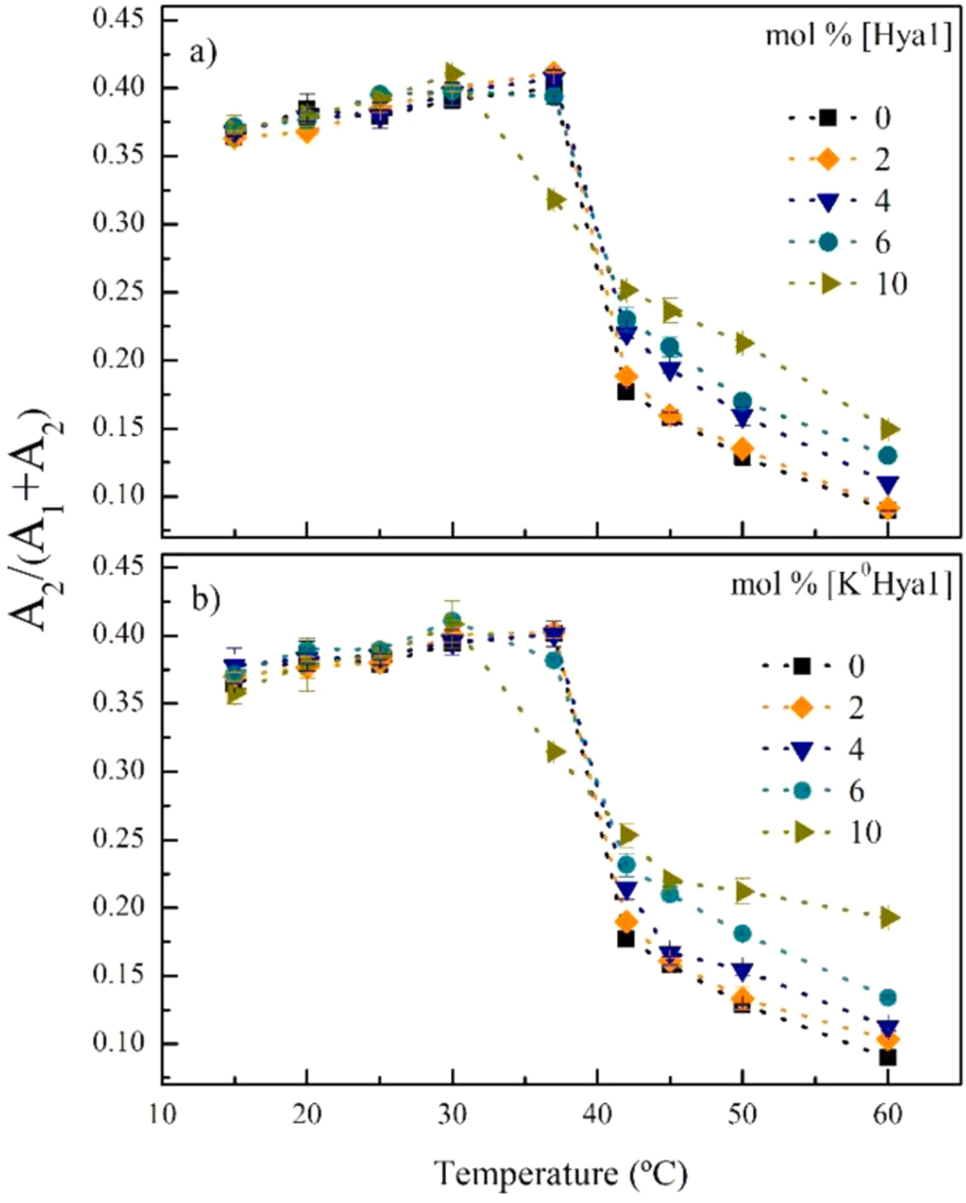


**Fig. 5.** The fraction of the area of the higher energy emission band ($A_2/(A_1 + A_2)$) as a function of the temperature for pure DPPG (black squares), and in the presence of Hya1 (Fig. 5a) or $K^0$Hya1 (Fig. 5b). Relative percentage of the peptides are: 2 mol% (orange diamonds), 4 mol% (blue down triangles), 6 mol% (dark cyan circles), and 10 mol% (dark yellow right triangles). (For interpretation of the references to colour in this figure legend, the reader is referred to the web version of this article.)

charged analogue.

To better understand and quantify the effects of the two peptides on the Laurdan emission, we transformed the Laurdan emission spectra from wavelength to energy, as described in Section 2.6 and decomposed it into two Gaussian bands: $A_1$ and $A_2$ are the areas of the Gaussian bands of lower and higher energy, respectively (see Fig. SM3). The relative contribution of the area of the most energetic band ($A_2$) of the Laurdan fluorescence emission to the total spectrum, $A_2/(A_1 + A_2)$, is plotted as a function of the temperature, for the different concentrations of the two peptides (Fig. 5). The relative fraction of the area of the Gaussian band seems to be an appropriate parameter to monitor the changes induced by the peptides on the membrane, since the positions of the Gaussian bands are not much affected by the peptides (Fig. SM7), maybe apart from those relative to the highest peptide concentration used here (10 mol%). But that is possibly a subject for further investigation (see, for instance, De Vequi-Suplicy et al., 2006).

In the gel phase, from 15 ºC to 30 ºC, the relative area ($A_2$) is nearly unaffected by the increase of the temperature. In fact, at temperatures from 15 ºC to 30 ºC, Laurdan emission from gel DPPG vesicles is almost constant, see Fig. SM8. A similar behavior was observed for Laurdan emission from gel 1,2-dipalmitoyl-sn-glycero-3-phosphocholine (DPPC) vesicles (Masukawa et al., 2019). In the fluid phase, at temperatures above 39 ºC, the contribution of the most energetic band decreases indicating that Laurdan is probing the bilayer fluidification induced by the temperature rise (Fig. 5a and b).

Above 39 °C, in fluid DPPG, as the peptide concentration increases, the contribution of the higher energy emission band $A_2$ increases, as compared to pure DPPG membranes, indicating that the vicinity of

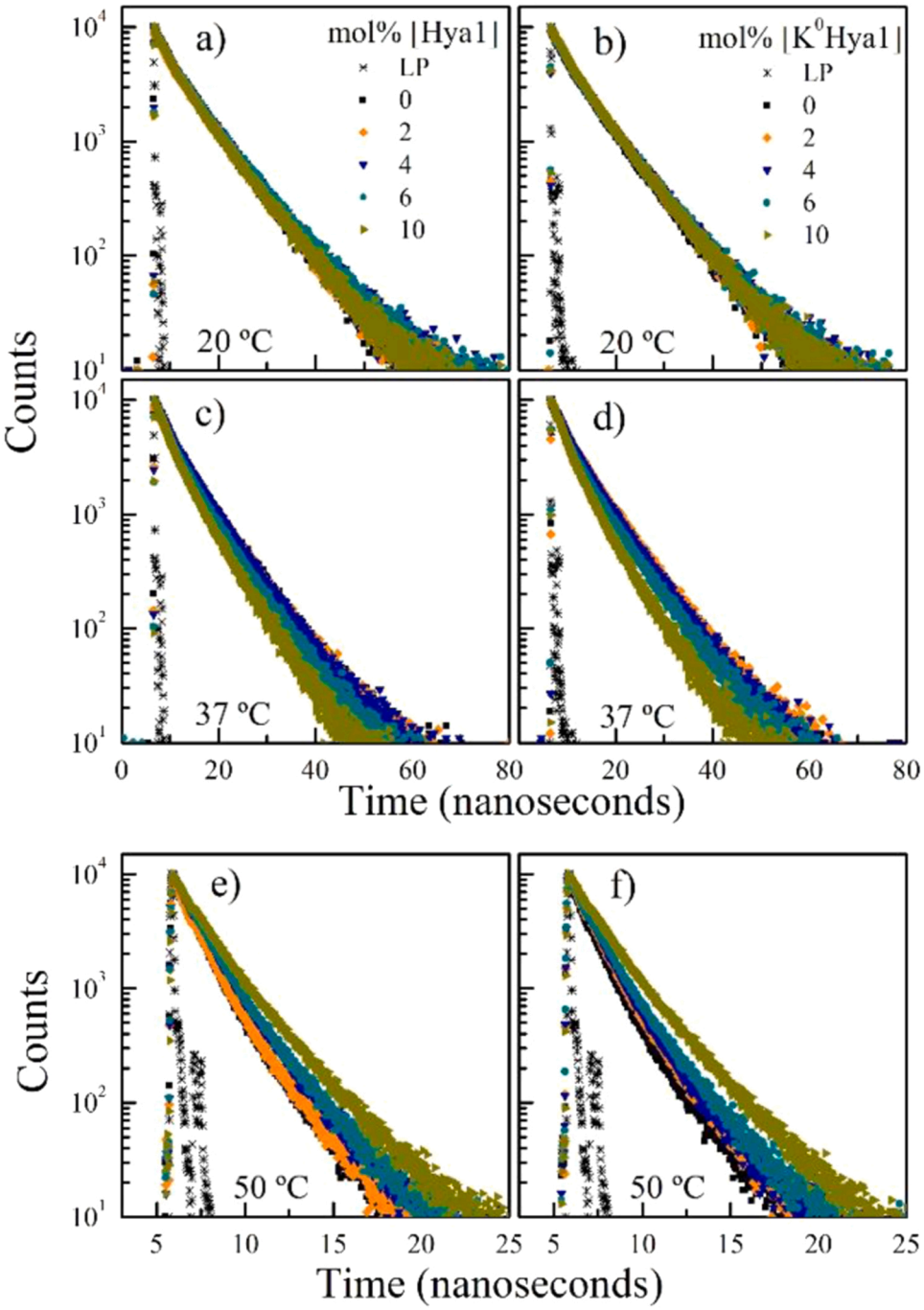


**Fig. 6.** Laurdan fluorescence decay incorporated into DPPG (500 μmol $L^{-1}$) vesicles in the absence (black squares) and with different concentrations of Hya1 (left column) or $K^0$Hya1 (right column), at three temperatures, 20 ºC (a, b), 37 ºC (c,d), and 50 ºC (e,f). Relative percentage of the peptides: 2 mol% (orange diamonds), 4 mol% (blue down triangles), 6 mol % (dark cyan circles), and 10 mol% (dark yellow right triangles). *LP is the laser profile. Excitation light at 284 nm and emission at 428 nm. (For interpretation of the references to colour in this figure legend, the reader is referred to the web version of this article.)

Laurdan becomes more packed, with higher restriction of motion and/or lower polarity.

We would like to call attention to the data at 37 ºC. At that temperature, different from pure DPPG membrane, some of the DPPG samples with peptide have already undergone the gel-fluid transition as revealed by DSC (see red dashed line in Fig. 2). For instance, at 10 mol% of both peptides, with the samples mostly in the fluid phase (Fig. 2), there is a clear decrease on the percentage of the higher energy emission band $A_2$, in accord with Laurdan monitoring a fluid membrane (dark yellow right triangles in Fig. 5a and b).

Though calorimetric measurements show significant differences induced by Hya1 and $K^0$Hya1 on DPPG membranes (Figs. 2 and 3), Laurdan emission from fluid liposomes in the presence of both peptides are very similar (Fig. 5). Note, for instance, that Laurdan fluorescence is not sensitive to the presence of the two different membrane regions indicated by DSC to coexist in the presence of 3–6 mol% of $K^0$Hya1 (see Fig. 2b). The change on Laurdan fluorescence for those samples (Fig. 5b) indicates that Laurdan is probing the peptide-rich region. Namely, at least part of the probe partitions into the peptide-rich area, otherwise its fluorescence spectrum would not change for $K^0$Hya1 concentrations up to 6 mol%.

### 3.2.2. *Time-resolved fluorescence spectroscopy*

Time-resolved fluorescence spectroscopy is a technique to determine the fluorescent lifetime, *i. e.*, the time between the excitation and emission of the fluorophore. Fluorescent lifetimes have little dependence on fluorophore emission intensity, being a good approach to investigate molecules when the light scattering is significantly high (Santos et al., 2003).

We measured Laurdan decay embedded into DPPG vesicles in the absence and in the presence of both peptides. All the decay curves (Fig. 6) could be well fitted with two exponential decays (see Eq. 2). As expected, the lifetimes at higher temperatures are smaller in comparison with those found at 20 ºC (see Fig. 7). This is due to the increase of non-radiative decay processes as temperature increases (Lakowicz, 2006). Similar to the state-steady fluorescence experiments discussed above, Laurdan decay in gel DPPG vesicles was not much affected by increasing amount of the peptides, (Fig. 6a and b), whereas Laurdan decay in fluid DPPG was strongly affected by increasing concentration of both peptides (Fig. 6e and f). We would like to stress that, as observed with steady-state experiments, Laurdan decays at 37 ºC (Fig. 6c and d), probe the undergone gel-fluid transition induced by high contents of peptides, 6 and 10 mol%, (Fig. 2).

The longer Laurdan lifetime ($\tau_2$) was more sensitive to changes in the lipid structure/dynamics induced by the peptides. Therefore, we plotted $\tau_2$, and its respective fractional contribution ($f_2$), versus the temperature, in the presence of different amounts of Hya1 (Fig. 7a and c) and $K^0$Hya1 (Fig. 7b and d).

Similar to the results obtained with steady-state fluorescence, Laurdan lifetimes were found quite insensitive to the binding of the peptides to gel phase DPPG (see Fig. 7 for temperatures below 30 °C). Considering that the fluorescence quantum yield ($\Phi$) is correlated to the rate of radiative decay ($k_r$) and the fluorophore's lifetime ($\tau$) by $\Phi = k_r\,\tau$, and assuming that $k_r$ is constant (Valeur, 2002), it is possible to conclude that neither the balance between the two emissions of Laurdan (Fig. 5), nor the fluorescence quantum yield (Fig. SM8) and lifetimes, are sensitive to possible changes caused by the peptides on gel DPPG.

On the other hand, Laurdan was found to be quite sensitive to changes induced by the peptides in fluid DPPG. The presence of both

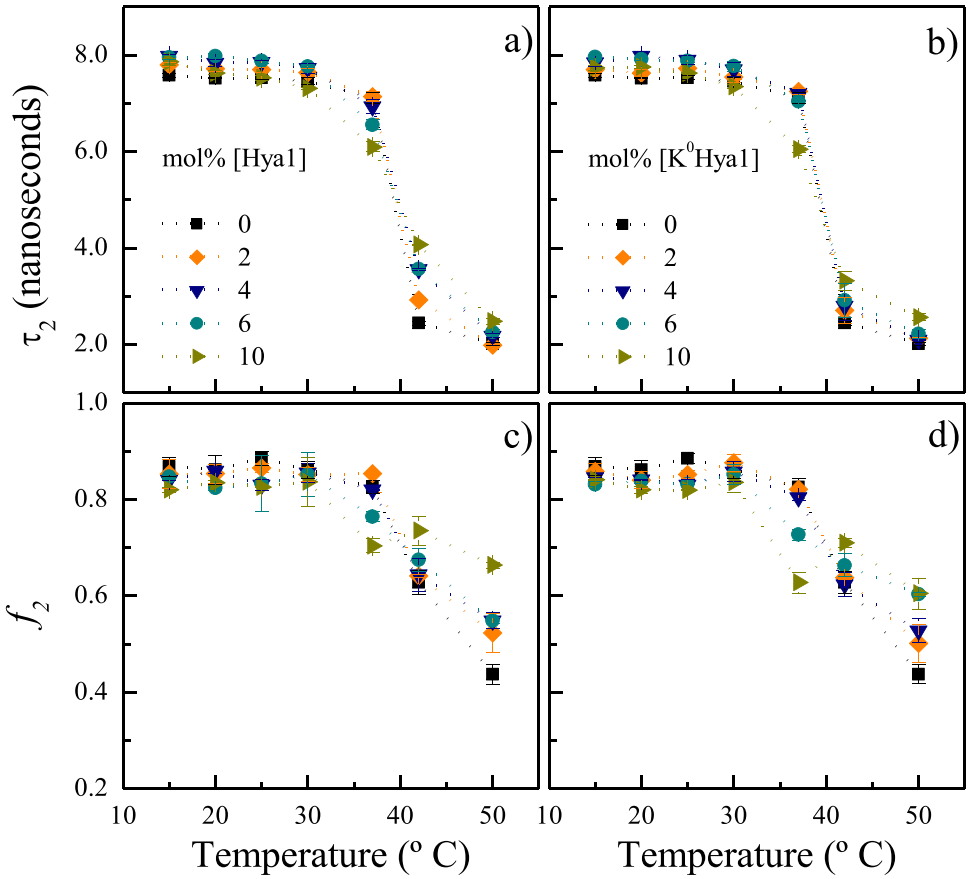


**Fig. 7.** Longer Laurdan lifetime (a,b) and its fraction contribution (c,d), as a function of the temperature, in the presence of different amounts of Hya1 (a,c) and $K^0$Hya1 (b,c). Error bar indicates standard deviation of at least three experiments with different samples. If not shown, the deviation was found to be smaller than the symbol.

peptides enhanced the longer Laurdan fluorescent lifetime (see 40 ºC and 50 °C in Fig. 7a and b), indicating that the vicinity of Laurdan is changed by the peptides, becoming more packed and/or less hydrated in comparison with pure DPPG vesicles. The fraction contribution of the longer lifetime ($f_2$) follows the same behavior of that found for $\tau_2$. As the longer lifetime is associated with the decay from the higher energy state (Vequi-Suplicy et al., 2015), that is supporting the data obtained with steady-state fluorescence, where the decomposition of the fluorescence spectrum indicated an increase of the percentage of the higher energy state as the amount of peptide increases (see Fig. 5).

### 3.3. ESR of spin labels incorporated into DPPG membranes

Spin labels are sensitive to lipid packing, lipid phase transition, and viscosity of their nano-environment (Marsh., 1981). By using the spin label 5-PCSL, we monitored changes in the bilayer nanostructure and dynamics at the level of the 5th carbon of the acyl chain, that is, at the vicinity of the DPPG glycerol backbone, close to the location where Laurdan is supposed to reside when incorporated into lipid bilayers (Parasassi et al., 1998; De Vequi-Suplicy et al., 2006; Jurkiewicz et al., 2006). Since, Laurdan emission in gel liposomes was little affected by the presence of both peptides, we considered important to investigate with other techniques if gel DPPG bilayer structure and/or dynamics were modified by the peptides.

Fig. 8 shows the ESR spectra of 5-PCSL incorporated into gel (left column) and fluid DPPG vesicles (right column) in the absence (black lines) and with increasing amounts of Hya1 (orange lines) and $K^0$Hya1 (blue lines).

The modifications induced in the ESR spectra by the peptides are not visually evident (Fig. 8), but they can be quantified by experimental parameters directly measured on the 5-PCSL ESR spectra, as described in Section 2.8. For gel DPPG liposomes, we plotted the maximum hyperfine splitting ($2A_{max}$) as a function of the temperature (Fig. 9), in the absence (black squares) and in the presence of increasing amounts of Hya1 (Fig. 9a) or $K^0$Hya1 (Fig. 9b).

$2A_{max}$ provides information about the anisotropy and the dynamics of the probe, that is, the viscosity of the nanoregion in which the probe is embedded. Higher $A_{max}$ values are related to higher restriction of the mobility of the spin label. Note that $A_{max}$ decreases (Fig. 9) as the temperature increases, showing that even in the membrane gel phase the increase of temperature leads to a relative fluidification of the bilayer. Interesting to point out that, as discussed above, Laurdan is insensitive to those alterations (see Fig. SM8).

ESR experiments reveal that both peptides bind to gel DPPG membranes, turning the membrane even more rigid and/or organized, as indicated by the increasing of the $A_{max}$ parameter as the peptide concentration increases. That evinces that, indeed, Laurdan has low sensitivity to changes induced on gel DPPG membranes.

Fig. 9 displays different patterns concerning the alterations induced by Hya1 and $K^0$Hya1 on DPPG membranes. Whereas for Hya1 the gel membrane shows to be progressively rigidified by increasing amounts of the peptide (progressive increase of $A_{max}$, Fig. 9a), for $K^0$Hya1 there is a clear jump between 4 and 6 mol% of the peptide (Fig. 9b). Interesting to observe that for this more positively charged peptide, DSC traces strongly indicate that up to 5 mol% there is a clear coexistence of two regions in the bilayer, as discussed above: peptide rich and peptide free regions (see Fig. 3b). For 6 mol% of $K^0$Hya1, and above, there is not much bulk lipid domains left. Accordingly, for $K^0$Hya1, up to 4 mol%, the spin probe 5-PCSL would preferentially partition in the more fluid domains of bulk lipids (see Fig. 9b). In the literature, it is possible to find reports indicating that spin probes can preferentially partition in more fluid environments in a membrane (see, for instance, Temprana et al., 2012, and references therein). It is important to note, nevertheless, that both peptides rigidify gel DPPG liposomes. At concentrations of 6 and 10 mol%, $K^0$Hya1 displays a stronger effect.

Hence, the ESR data in Fig. 9 reinforce our hypothesis that, contrarily

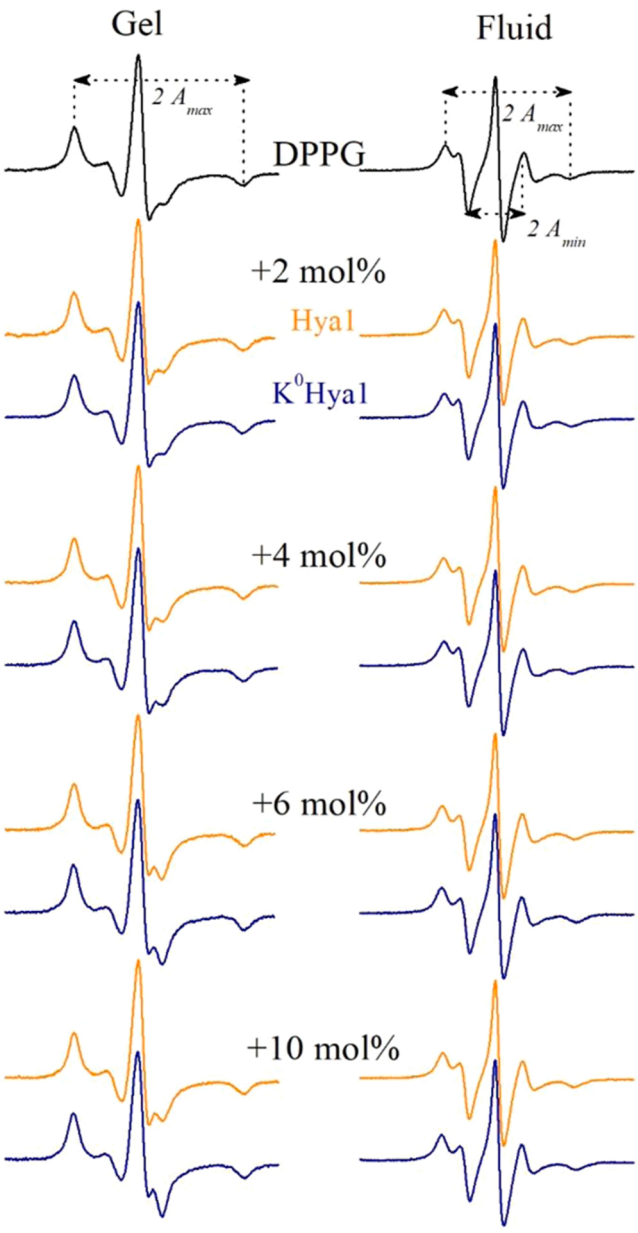


**Fig. 8.** Typical ESR spectra of 5-PSCL embedded into 3 mmol $L^{-1}$ of DPPG vesicles in the gel (20 ºC, left column) or in the fluid phase (45 ºC, right column) in the absence (black lines), and with increasing amounts of Hya1 (orange lines), and $K^0$Hya1 (blue lines). Relative percentage of the peptides from top to bottom: 2 mol%, 4 mol%, 6 mol%, and 10 mol%. The total spectra width is 100 Gauss. The maximum ($2A_{max}$) and minimum ($2A_{min}$) hyperfine splitting are indicated in the figure. (For interpretation of the references to colour in this figure legend, the reader is referred to the web version of this article.)

to Hya1, $K^0$Hya1 binds so strongly to the membrane that the molecule does not diffuse on the membrane, giving rise to peptide-rich and peptide-free regions, for low peptide concentrations.

To assess the modifications induced by the AMPs on fluid DPPG membranes, we calculated the effective order parameter, $S_{eff}$ (Eq. 3). $S_{eff}$ provides information about lipid order/mobility at the level of the 5th carbon atom: when all probe molecules are completely oriented parallel to the bilayer normal, $S_{eff}$ is equal to unity. On the other hand, when $S_{eff}$ values are close to zero the spin probe is in rapid, isotropic, and wobbly motion, indicating a quite loose environment (see Rozenfeld et al., 2017, and references therein).

Fig. 10 displays $S_{eff}$ values as a function of the temperature for 5-

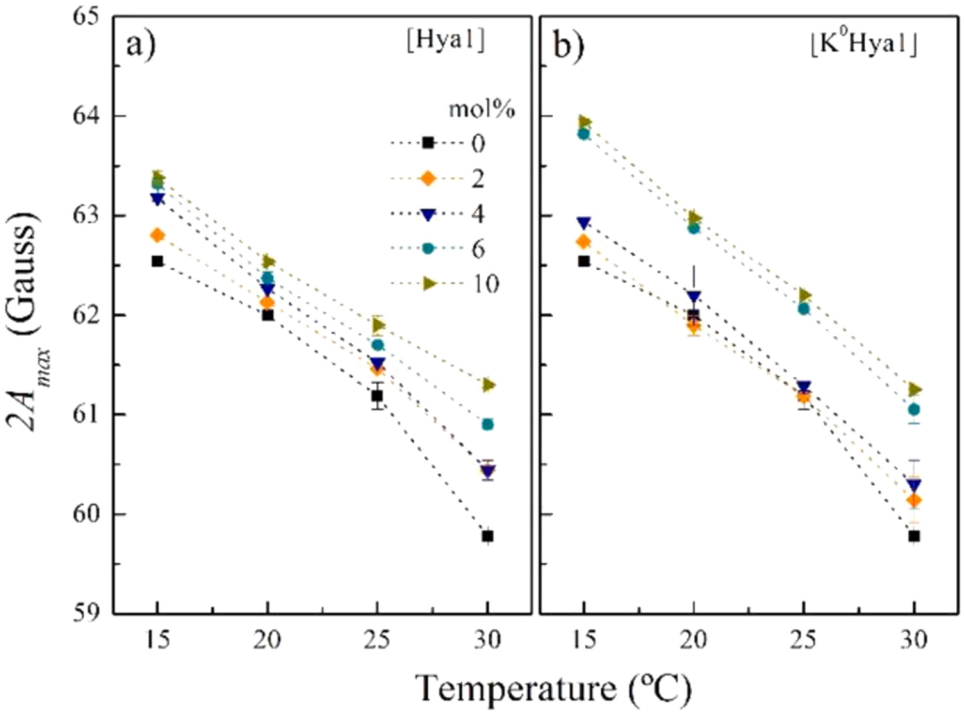


**Fig. 9.** Temperature dependence of the outer hyperfine splitting ($2A_{max}$) measured on the ESR spectrum of 5-PSCL embedded into 3 mmol $L^{-1}$ gel liposomes of DPPG. The data were obtained in the absence of AMPs (black square), and in the presence of Hya1 (a) or $K^0$Hya1 (b). The relative percentages of AMPs were 2 mol% (orange diamonds), 4 mol% (blue down triangles), 6 mol% (dark cyan circle), and 10 mol% (dark yellow right triangle). Error bar indicates standard deviation of at least three experiments with different samples. If not shown, the deviation was found to be smaller than the symbol. (For interpretation of the references to colour in this figure legend, the reader is referred to the web version of this article.)

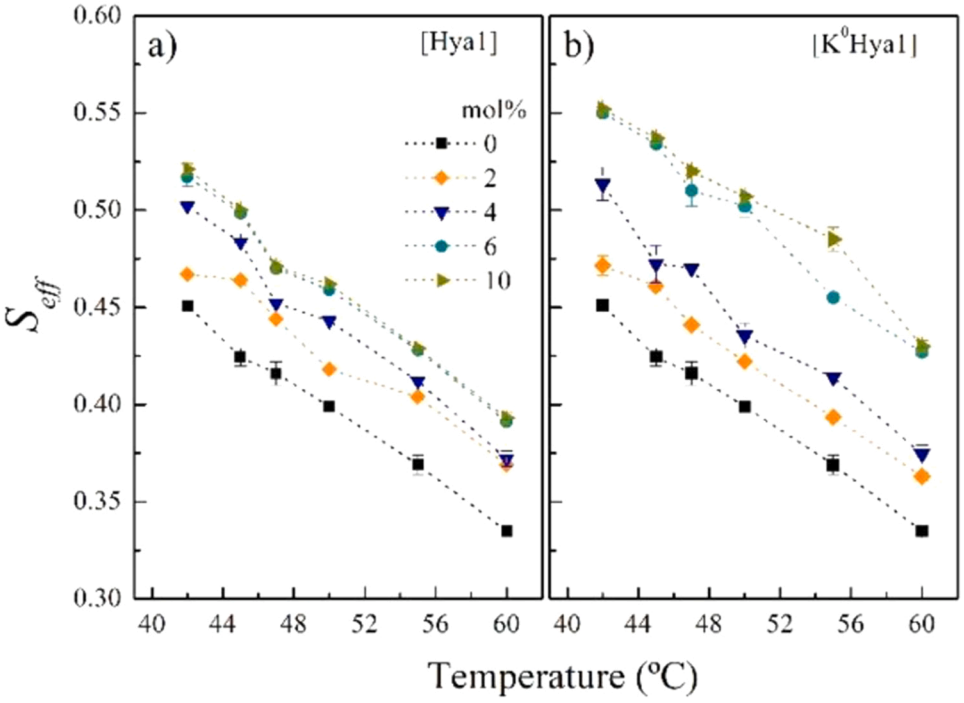


**Fig. 10.** Temperature dependence of the effective order parameter, $S_{eff}$, measured on ESR spectra of 5-PCSL incorporated into 3 mmol $L^{-1}$ of fluid liposomes of DPPG. The data were obtained in the absence of AMPs (black squares), and in the presence of Hya1 (a) and $K^0$Hya1 (b). The relative percentages of AMPs were 2 mol% (orange diamonds), 4 mol% (blue down triangles), 6 mol% (dark cyan circle), and 10 mol % (dark yellow right triangle). Error bar indicates standard deviation of at least three experiments with different samples. If not shown, the deviation was found to be smaller than the symbol. (For interpretation of the references to colour in this figure legend, the reader is referred to the web version of this article.)

PCSL incorporated in fluid DPPG liposomes in the absence and with increasing concentrations of Hya1 (Fig. 10a) and $K^0$Hya1 (Fig. 10b).

The increase of the temperature induces higher lipid motion on pure DPPG bilayer, decreasing $S_{eff}$ values (see black squares in Fig. 10). Increasing amounts of Hya1 (Fig. 10a) induces a progressive increase in $S_{eff}$ values with a saturation around 6 mol%. The presence of the most cationic peptide $K^0$Hya1 also enhances $S_{eff}$ values, however, the gap between 4 and 6 mol% data is also observed here, for the fluid phase of the membrane. This is a strong indication of the presence of the two domains even in fluid DPPG membranes: peptide rich and peptide free domains, as discussed above.

Moreover, $K^0$Hya1 seems to be more effective in organizing fluid DPPG bilayers than the native peptide, since $S_{eff}$ values found for the two peptides, at the same peptide concentration, are always higher for $K^0$Hya1. This result is in accord with the DSC thermograms, which show that, at the highest peptide concentration used here (10 mol%), the interaction between $K^0$Hya1 and DPPG yielded a more cooperative thermal-transition peak than that found for the interaction between

Hya1 and DPPG (Fig. 2).

### 3.4. CF entrapped in DPPG LUVs: leakage assay

CF leakage assay is an efficient technique to monitor if a foreign molecule can change the structure of liposomes, forming pores, either stable or transient. As previously stated, CF is a dye that when entrapped within liposomes at 50 mmol $L^{-1}$ is almost non-fluorescent, due to self-quench. If a given molecule disrupts the bilayer, causing permanent or temporary pores, allowing the dye to leak into the bulk, its dilution will yield an increase on the CF emission intensity.

By using this methodology, we investigated if 8 mol% of the AMPs could induce pore formation on anionic vesicles composed of DPPG at the gel phase, at 25 °C. Moreover, to mimic DPPG fluid phase at 25 °C, the unsaturated lipid POPG ((1-palmitoyl-2-oleoyl- *sn*-glycero-3-phospho-(1′-*rac*-glycerol)) was used. The use of POPG was necessary due to the difficulties of performing the leakage experiment with DPPG at higher temperatures (see Enoki et al., 2018). That peptide concentration was chosen because above 6 mol% the two peptides appear to be homogeneously distributed on the DPPG membrane, with no coexistence of different domains (see Fig. 2).

The control consists of DPPG (Fig. 11a and 11c) or POPG (Fig. 11b and 11d) vesicles containing CF in the absence of peptides (gray dotted lines in Fig. 11). The spontaneous CF leakage was found to be negligible for gel DPPG vesicles (less than 3% in 2000 s), whereas fluid POPG vesicles (Fig. 3d) display an acceptable spontaneous leakage around 20% within 30 min, as previously reported (Enoki et al., 2018). Fig. 11a shows that both peptides (8 mol%) can induce CF leakage on gel DPPG

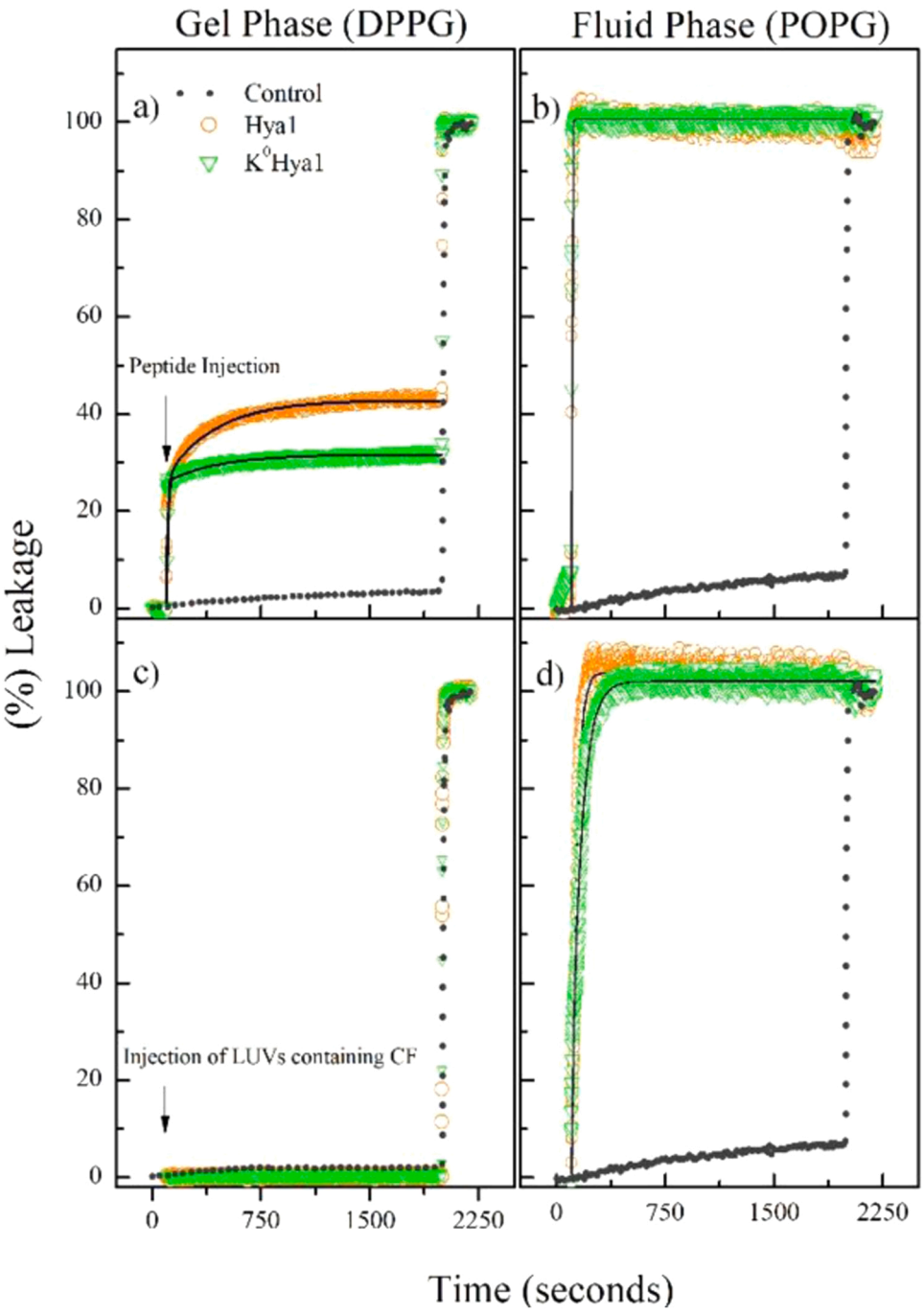


**Fig. 11.** Typical kinetics of CF leakage through LUVs composed of gel DPPG (a), and fluid POPG (b) membranes, in the presence of 8 μmol $L^{-1}$ of Hya1(red circles) or $K^0$Hya1 (green down triangles). Black lines indicate the fittings according to Eq. 5. Kinetic curves of CF leakage through LUVs composed of gel DPPG (100 μmol $L^{-1}$) (c) and fluid POPG (d) in the presence of gel DPPG (c) and fluid POPG (d) dispersions (100 μmol $L^{-1}$) pre-incubated with 8 μmol $L^{-1}$ of Hya1(red circles) or $K^0$Hya1 (green down triangles) for 33 min. The experiments were performed at 25 °C. (For interpretation of the references to colour in this figure legend, the reader is referred to the web version of this article.)

liposomes (Fig. 11a). It is very interesting that the effect of Hylin peptides on fluid PG vesicles is much more dramatic (POPG in Fig. 11b), at the same peptide concentration: both peptides rapidly caused total CF release from POPG vesicles.

Due to the quick CF-leakage, we considered important to check the integrity of the vesicles. By using dynamic light scattering (DLS), the hydrodynamic radius of gel and fluid vesicles was monitored as a function of the peptide concentration (Fig. SM9). The vesicles do not collapse due to the peptide action. However, the vesicle average size increases (Fig. SM9), suggesting that the Hylin peptides may cause some vesicle fusion or aggregation.

As found for many CF-leakage experiments (Almeida and Pokorny, 2010; Enoki et al., 2018) the kinetics with DPPG vesicles could be well fitted by two exponentials (Eq. 5; black lines in Fig. 11a), indicating two kinetic processes, with different decay times, a shorter ($T_1$) and a longer ($T_2$) time constant (Table 1). For the experiments with fluid POPG liposomes, any fitting of the data would be quite inaccurate, as the CF-kinetics curves are nearly composed of two straight lines. Therefore, Table 1 only exhibits the values of the best fitting parameters obtained for gel DPPG CF-release kinetics.

The CF release processes induced by the two peptides in gel DPPG vesicles were found to be different, particularly the first process, corresponding to the short times (Table 1 and Fig. SM10). $T_1$ value for the more positively charged peptide, $K^0$Hya1, was found to be about six times shorter than that found for the native peptide (Table 1), indicating a much faster reaction. That could either be related to the structural modifications this peptide causes on the bilayer or to its faster binding on anionic PG bilayers. Interestingly, the total percentages of leakage due to the first process are very similar for the two peptides, around 26% (see $A_1$ values in Table 1).

The longer process yielded very similar $T_2$ values, indicating that both peptides caused similar residual CF leakages. Furthermore, the total leakage caused by the peptides ($A_1 + A_2$) was found to be somewhat higher for the native peptide as compared with $K^0$Hya1 (Table 1).

The total leakage caused by the peptides on DPPG vesicles, at the used concentration, ($A_1 + A_2$), is far from 100% (42% and 33%, for Hya1 and $K^0$Hya1, respectively, Table 1), value that would be expected if CF had leaked from all DPPG vesicles. That result has been found for several antimicrobial peptides, and it is still a subject of discussion in the literature (see Enoki et al., 2018, and references therein). For instance, it has been speculated that a certain amount of peptide-bound per vesicle would be necessary for triggering the opening of pores, related to peptide-peptide interaction on the membrane. Hence, the CF leakage would not be complete until all vesicles reach this value (Gregory et al., 2008; Wimley, 2010).

As both peptides were unable to induce complete CF release from DPPG LUVs, (see ($A_1 + A_2$) values in Table 1), we designed a second experiment based on CF-leakage to address this effect, according to the experiments discussed by Sani et al. (2014), to answer the following question: do the Hylin peptides get strongly attached to some DPPG vesicles therefore being unable to migrate and interact with other DPPG vesicles? To answer this question, we incubated the peptides with pure DPPG (Fig. 11c) or POPG (Fig. 11d) vesicles, without CF, for 2000 s, under the same conditions of the first CF leakage assay (Fig. 11a and b). Then, we started the fluorescence measurement, adding DPPG (Fig. 11c) or POPG (Fig. 11d) vesicles loaded with CF at the 100th second.

Note that, at the concentration used here, the peptides preincubated with DPPG liposomes do not promote any significant CF release on the new DPPG vesicles added to the sample (Fig. 11c), thus indicating that, at 8 mol%, both peptides are strongly attached to the DPPG bilayer. Namely, the peptide concentration in solution is not enough to cause CF release in the newly added DPPG vesicles.

Opposite to that, at the same peptide concentration, the samples with peptides preincubated with fluid POPG could rapidly promote complete CF release from the newly added POPG vesicles. It is noteworthy, that it has been observed that Hylin peptides are much more effective to induce pore formation in fluid than in gel vesicles (Vignoli Muniz et al., 2020; Enoki et al., 2018). Thus, it seems that it is necessary only a small concentration of peptides to visit and interact with fluid PG vesicles to induce pore formation on the liposomes. The study of this phenomenon is out of the scope of the present work, and deserves further investigation.

**Table 1**
Fitting parameters of the data in Fig. 11(a) using Eq. 5. The peptide net charge is shown in parenthesis.

| AMP | $A_1$ | $T_1(s)$ | $A_2$ | $T_2(s)$ | $A_1 + A_2$ |
|---|---|---|---|---|---|
| **Hya1 (+3)** | (27 ± 2) | (9.9 ± 0.3) | (15 ± 3) | (340 ± 7) | (42 ± 3) |
| **$K^0$Hya1 (+4)** | (26 ± 3) | (1.53 ± 0.05) | (7 ± 2) | (346 ± 5) | (33 ± 3) |

## 4. Conclusions

This work shows that the native Hylin a1 and its more positively charged analogue, $K^0$Hya1, strongly interact with negatively charged PG bilayers. However, the extra positive lysine residue, at the beginning of the analogue chain, makes a difference on the effects caused by the peptide on the membrane.

DSC thermograms strongly indicate that $K^0$Hya1, up to 6 mol%, induces the coexistence of regions of peptide-rich and peptide-poor on DPPG bilayers, whereas the native peptide seems to cause a space-average and/or time-average disruption on the membrane. This hypothesis is supported by the data obtained with a spin probe close to the bilayer surface (5-PCSL).

The ESR spectra obtained with the spin probe (5-PCSL), and the leakage experiments with CF, show that the two peptides disrupt both gel and fluid phases of PG membranes. The large molecule of CF was shown to leak through permanent or temporarily pores on gel and fluid PG membranes in the presence of 8 mol% of the peptides, whereas the effect on fluid POPG was found to be much more dramatic causing rapid and complete CF release. However, the Laurdan fluorescent probe was unable to detect any change caused by the peptides on the gel phase of DPPG. Accordingly, this work makes evident that Laurdan is not an appropriate membrane probe for lipid bilayers in the gel state. Moreover, the spin label could detect relevant differences on the structural effect the two peptides cause on PG membranes, which could not be detected by Laurdan fluorescence.

The leakage experiments show that both peptides strongly bind to gel DPPG vesicles, possibly through electrostatic interaction, with very low partition in the water medium. Hence, they are unable to cause leakage, or to disrupt, newly added DPPG vesicles to the dispersion. Interestingly, the peptides preincubation with fluid PG membranes did not prevent the peptides to cause CF release from newly added fluid PG vesicles, possibly suggesting that only a small amount of Hylin peptides in solution is necessary to induce pore formation in fluid PG membranes.

Our results reveal how different approaches provide different information about modifications induced by exogenous molecules on a membrane bilayer structure, and may help to better understand the mechanisms of action of Hylin a1 peptides on anionic membranes, models for prokaryotic cells.

## Acknowledgment

This work was supported by the Brazilian agencies CNPq and FAPESP (2017/25930–1 and 2021/01593–1). M.T.L. and E.M.C. are recipients of CNPq research fellowships. G.S.V.M., E.L.D. and M.T.L. acknowledge support from the National Institute of Science and Technology Complex Fluids (INCT-FCx), financed by CNPq (141260/2017–3) and FAPESP (2014/50983–3 and 2018/20162–9). The authors thank Karin A. Riske and Katia R. Perez for important discussions concerning the leakage assays.

## Appendix A. Supporting information

Supplementary data associated with this article can be found in the online version at doi:10.1016/j.chemphyslip.2022.105173.

## References


Molecular biology of the cell. In: Alberts, B. (Ed.), 2008. Garland Science, New York, fifth ed.

Almeida, P.F., Pokorny, A., 2010. Antimicrobial peptides, chapter 11, binding and permeabilization of model membranes by amphipathic peptides. In: Giuliani, A., Rinaldi, A.C. (Eds.), Antimicrobial Peptides: Methods and Protocols. Humana Press/Springer, New York.

Alves, E.S., Junior, E.C., Cilli, E.M., Castro, M.S., Fontes, W., de Magalhães, M.T., Lião, L. M., de Oliveira, A.L., 2015. Micelle bound structure and model membrane interaction studies of the peptide Hylin a1 from the arboreal south american frog *Hypsiboas albopunctatus*. PPL 22, 719–726. https://doi.org/10.2174/0929866522666150610092657.

Bacalum, M., Zorilă, B., Radu, M., 2013. Fluorescence spectra decomposition by asymmetric functions: Laurdan spectrum revisited. Anal. Biochem. 440, 123–129. https://doi.org/10.1016/j.ab.2013.05.031.

Bransden, B.H., Joachain, C.J., 1986. Physics of Atoms and Molecules. Longman, London, New York.

Brogden, K.A., 2005. Antimicrobial peptides: pore formers or metabolic inhibitors in bacteria? Nat. Rev. Microbiol. 3, 238–250. https://doi.org/10.1038/nrmicro1098.

Castro, M.S., Ferreira, T.C., Cilli, E.M., Crusca E, Jr, Mendes-Giannini, M.J., Sebben, A., Ricart, C.A., Sousa, M.V., Fontes, W., 2009. Hylin a1, the first cytolytic peptide isolated from the arboreal South American frog Hypsiboas albopunctatus ("spotted treefrog"). Peptides 30, 291–296. https://doi.org/10.1016/j.peptides.2008.11.003.

Chessa, C., Bodet, C., Jousselin, C., Wehbe, M., Lévêque, N., Garcia, M., 2020. Antiviral and immunomodulatory properties of antimicrobial peptides produced by human keratinocytes. Front. Microbiol. 11, 1155. https://doi.org/10.3389/fmicb.2020.01155.

Crusca E, Jr, Câmara, A.S., Matos, C.O., Marchetto, R., Cilli, E.M., Lião, L.M., Lima de Oliveira, A., 2017. NMR structures and molecular dynamics simulation of hylin-a1 peptide analogs interacting with micelles. J. Pept. Sci. 23, 421–430. https://doi.org/10.1002/psc.3002.

Crusca E, Jr, Rezende, A.A., Marchetto, R., Mendes-Giannini, M.J., Fontes, W., Castro, M. S., Cilli, E.M., 2011. Influence of N-terminus modifications on the biological activity, membrane interaction, and secondary structure of the antimicrobial peptide hylin-a1. Biopolymers 96, 41–48. https://doi.org/10.1002/bip.21454.

Datta, S., Roy, A., 2021. Antimicrobial peptides as potential therapeutic agents: a review. Int. J. Pept. Res. Ther. 27, 555–577. https://doi.org/10.1007/s10989-020-10110-x.

De Vequi-Suplicy, C.C., Benatti, C.R., Lamy, M.T., 2006. Laurdan in fluid bilayers: position and structural sensitivity. J. Fluoresc. 16, 431–439. https://doi.org/10.1007/s10895-005-0059-3.

Prokaryotic Antimicrobial. In: Drider, D., Rebuffat, S. (Eds.), 2011. Peptides. Springer, New York, New York, NY.

Enoki, T.A., Henriques, V.B., Lamy, M.T., 2012. Light scattering on the structural characterization of DMPG vesicles along the bilayer anomalous phase transition. Chem. Phys. Lipids 165, 826–837. https://doi.org/10.1016/j.chemphyslip.2012.11.002.

Enoki, T.A., Moreira-Silva, I., Lorenzon, E.N., Cilli, E.M., Perez, K.R., Riske, K.A., Lamy, M.T., 2018. Antimicrobial peptide $K^{0}$-$W^{6}$-Hya1 induces stable structurally modified lipid domains in anionic membranes. Langmuir 34, 2014–2025. https://doi.org/10.1021/acs.langmuir.7b03408.

Freedman, D.H., 2019. Hunting for new drugs with AI. Nature 576, S49–S53. https://doi.org/10.1038/d41586-019-03846-0.

Gregory, S.M., Cavenaugh, A., Journigan, V., Pokorny, A., Almeida, P.F., 2008. A quantitative model for the all-or-none permeabilization of phospholipid vesicles by the antimicrobial peptide cecropin A. Biophys. J. 94, 1667–1680. https://doi.org/10.1529/biophysj.107.118760.

Heimburg, T., 2007. Thermal Biophysics of Membranes. Wiley-VCH Verlag, Weinheim.

Jurkiewicz, P., Olżyńska, A., Langner, M., Hof, M., 2006. Headgroup hydration and mobility of DOTAP/DOPC bilayers: a fluorescence solvent relaxation study. Langmuir 22, 8741–8749. https://doi.org/10.1021/la061597k.

Principles of fluorescence. In: Lakowicz, J.R. (Ed.), 2006. Spectroscopy. Springer, US, Boston, MA.

Lamy-Freund, M.T., Riske, K.A., 2003. The peculiar thermo-structural behavior of the anionic lipid DMPG. Chem. Phys. Lipids 122, 19–32. https://doi.org/10.1016/S0009-3084(02)00175-5.

Lúcio, A.D., Vequi-Suplicy, C.C., Fernandez, R.M., Lamy, M.T., 2010. Laurdan spectrum decomposition as a tool for the analysis of surface bilayer structure and polarity: a study with DMPG, peptides and cholesterol. J. Fluoresc. 20, 473–482. https://doi.org/10.1007/s10895-009-0569-5.

Marsh, D., 1981. Membrane spectroscopy. In: Grell, E. (Ed.). Springer Berlin Heidelberg, Berlin, Heidelberg.

Marsh, D., 2013. Handbook of Lipid Bilayers, second ed. CRC Press, Taylor & Francis Group, Boca Raton, FL.

Masukawa, M.K., Vequi-Suplicy, C.C., Duarte, E.L., Lamy, M.T., 2019. A closer look into laurdan as a probe to monitor cationic DODAB bilayers. J. Photochem. Photobiol. Chem. 376, 238–246. https://doi.org/10.1016/j.jphotochem.2019.03.006.

Mendonça, A., Rocha, A.C., Duarte, A.C., Santos, E.B.H., 2013. The inner filter effects and their correction in fluorescence spectra of salt marsh humic matter. Anal. Chim. Acta 788, 99–107. https://doi.org/10.1016/j.aca.2013.05.051.

Mingeot-Leclercq, Marie-Paule, Décout, Jean-Luc, 2016. Bacterial Lipid Membranes as Promising Targets to Fight Antimicrobial Resistance, Molecular Foundations and Illustration through the Renewal of Aminoglycoside Antibiotics and Emergence of Amphiphilic Aminoglycosides. MedChemComm 7 (4), 586–611. https://doi.org/10.1039/C5MD00503E.

Niko, Y., Didier, P., Mely, Y., Konishi, G., Klymchenko, A.S., 2016. Bright and photostable push-pull pyrene dye visualizes lipid order variation between plasma and intracellular membranes. Sci. Rep. 6, 18870. https://doi.org/10.1038/srep18870.

Ohmann, A., Li, C.-Y., Maffeo, C., Al Nahas, K., Baumann, K.N., Göpfrich, K., Yoo, J., Keyser, U.F., Aksimentiev, A., 2018. A synthetic enzyme built from DNA flips 107 lipids per second in biological membranes. Nat. Commun. 9, 2426. https://doi.org/10.1038/s41467-018-04821-5.

Pabst, Georg, Grage, Stephan L., Danner-Pongratz, Sabine, Jing, Weiguo, Ulrich, Anne S., Watts, Anthony, Lohner, Karl, Hickel, Andrea, 2008. Membrane Thickening by the Antimicrobial Peptide PGLa. Biophysical Journal 95 (12), 5779–5788. https://doi.org/10.1529/biophysj.108.141630.

Parasassi, T., De Stasio, G., Ravagnan, G., Rusch, R.M., Gratton, E., 1991. Quantitation of lipid phases in phospholipid vesicles by the generalized polarization of Laurdan fluorescence. Biophys. J. 60, 179–189. https://doi.org/10.1016/S0006-3495(91)82041-0.

Parasassi, T., Krasnowska, E.K., Bagatolli, L., Gratton, E., 1998. Laurdan and prodan as polarity-sensitive fluorescent membrane probes. J. Fluoresc. 8, 365–373. https://doi.org/10.1023/A:1020528716621.

Peetla, C., Stine, A., Labhasetwar, V., 2009. Biophysical interactions with model lipid membranes: applications in drug discovery and drug delivery. Mol. Pharm. 6, 1264–1276. https://doi.org/10.1021/mp9000662.

Phoenix, D., Dennison, S.R., Harris, F., 2013. Antimicrobial Peptides. Wiley-VCH, Weinheim.

Pizzolato-Cezar, L.R., Okuda-Shinagawa, N.M., Machini, M.T., 2019. Combinatory therapy antimicrobial peptide-antibiotic to minimize the ongoing rise of resistance. Front. Microbiol. 10. https://doi.org/10.3389/fmicb.2019.01703.

Prenner, E., Chiu, M., 2011. Differential scanning calorimetry: an invaluable tool for a detailed thermodynamic characterization of macromolecules and their interactions. J. Pharm. Bioallied. Sci. 3, 39–59. https://doi.org/10.4103/0975-7406.76463.

Raheem, N., Straus, S.K., 2019. Mechanisms of action for antimicrobial peptides with antibacterial and antibiofilm functions. Front. Microbiol. 10. https://doi.org/10.3389/fmicb.2019.02866.

Reinhardt, A., Neundorf, I., 2016. Design and application of antimicrobial peptide conjugates. Int. J. Mol. Sci. 17, 701. https://doi.org/10.3390/ijms17050701.

Riske, K.A., Barroso, R.P., Vequi-Suplicy, C.C., Germano, R., Henriques, V.B., Lamy, M.T., 2009. Lipid bilayer pre-transition as the beginning of the melting process. Biochim. Biophys. Acta BBA - Biomembr. 1788, 954–963. https://doi.org/10.1016/j.bbamem.2009.01.007.

Rivas, L., Luque-Ortega, J.R., Andreu, D., 2009. Amphibian antimicrobial peptides and Protozoa: Lessons from parasites. Biochim. Biophys. Acta BBA - Biomembr. 1788, 1570–1581. https://doi.org/10.1016/j.bbamem.2008.11.002.

Rouser, G., Siakotos, A.N., Fleischer, S., 1966. Quantitative analysis of phospholipids by thin-layer chromatography and phosphorus analysis of spots. Lipids 1, 85–86. https://doi.org/10.1007/BF02668129.

Rozenfeld, J.H.K., Duarte, E.L., Oliveira, T.R., Lamy, M.T., 2017. Structural insights on biologically relevant cationic membranes by ESR spectroscopy. Biophys. Rev. 9, 633–647. https://doi.org/10.1007/s12551-017-0304-4.

Rudrapal, M., Khairnar, J., G, S., Jadhav, A., 2020. Drug repurposing (DR): an emerging approach in drug discovery. In: Badria, A., F (Eds.), Drug Repurposing - Hypothesis, Molecular Aspects and Therapeutic Applications. IntechOpen.

Sani, M.-A., Gagne, E., Gehman, J.D., Whitwell, T.C., Separovic, F., 2014. Dye-release assay for investigation of antimicrobial peptide activity in a competitive lipid environment. Eur. Biophys. J. 43, 445–450. https://doi.org/10.1007/s00249-014-0970-0.

Sani, M.-A., Separovic, F., 2016. How membrane-active peptides get into lipid membranes. Acc. Chem. Res. 49, 1130–1138. https://doi.org/10.1021/acs.accounts.6b00074.

Santana, C.J.C., Magalhães, A.C.M., dos Santos Júnior, A.C.M., Ricart, C., Lima, B.D., Álvares, A., Freitas, S.M., Pires OR, Jr, Fontes, W., Castro, M.S., 2020. Figainin 1, a novel amphibian skin peptide with antimicrobial and antiproliferative properties. Antibiotics 9, 625. https://doi.org/10.3390/antibiotics9090625.

Santos, N.C., Prieto, M., Castanho, M.A.R.B., 2003. Quantifying molecular partition into model systems of biomembranes: an emphasis on optical spectroscopic methods. Biochim. Biophys. Acta BBA - Biomembr. 1612, 123–135. https://doi.org/10.1016/S0005-2736(03)00112-3.

Seddon, A.M., Casey, D., Law, R.V., Gee, A., Templer, R.H., Ces, O., 2009. Drug interactions with lipid membranes, 2509-19 Chem. Soc. Rev. 38. https://doi.org/10.1039/b813853m.

Takechi-Haraya, Y., Goda, Y., Sakai-Kato, K., 2018. Atomic force microscopy study on the stiffness of nanosized liposomes containing charged lipids. Langmuir 34, 7805–7812. https://doi.org/10.1021/acs.langmuir.8b01121.

Temprana, C.F., Duarte, E.L., Femia, A.L., Alonso Sdel, V., Lamy, M.T., 2012. Structural effect of cationic amphiphiles in diacetylenic photopolymerizable membranes. Chem. Phys. Lipids 165, 589–600. https://doi.org/10.1016/j.chemphyslip.2012.06.007.

Tornesello, A.L., Borrelli, A., Buonaguro, L., Buonaguro, F.M., Tornesello, M.L., 2020. Antimicrobial peptides as anticancer agents: functional properties and biological activities. Molecules 25, 2850. https://doi.org/10.3390/molecules25122850.

Valeur, B., 2002. Molecular Fluorescence: Principles and Applications. Wiley-VCH, Weinheim; New York.

Vequi-Suplicy, C.C., Coutinho, K., Lamy, M.T., 2015. New insights on the fluorescent emission spectra of Prodan and Laurdan. J. Fluoresc. 25, 621–629. https://doi.org/10.1007/s10895-015-1545-x.

Vequi-Suplicy, C.C., Orozco-Gonzalez, Y., Lamy, M.T., Canuto, S., Coutinho, K., 2020. A new interpretation of the absorption and the dual fluorescence of Prodan in solution. J. Chem. Phys. 153, 244104 https://doi.org/10.1063/5.0025013.

Vignoli Muniz, Gabriel, De la Torre, Lilia I., Duarte, Evandro L., Lorenzón, Esteban N., Cilli, Eduardo M., Balan, Andrea, Lamy, M. Teresa, 2020. Interaction of synthetic antimicrobial peptides of the Hylin a1 family with models of eukaryotic structures: Zwitterionic membranes and DNA. Biochemistry and Biophysics Reports. https://doi.org/10.1016/j.bbrep.2020.100827.

Vignoli Muniz, G.S., Souza, M.C., Duarte, E.L., Lamy, M.T., 2021. Comparing the interaction of the antibiotic levofloxacin with zwitterionic and anionic membranes: calorimetry, fluorescence, and spin label studies. Biochim. Biophys. Acta BBA - Biomembr. 1863, 183622 https://doi.org/10.1016/j.bbamem.2021.183622.

Wang, G., Li, X., Wang, Z., 2016. APD3: the antimicrobial peptide database as a tool for research and education. Nucleic Acids Res. 44, D1087–D1093. https://doi.org/10.1093/nar/gkv1278.

Weber, G., Farris, F.J., 1979. Synthesis and spectral properties of a hydrophobic fluorescent probe: 6-propionyl-2-(dimethylamino)naphthalene. Biochemistry 18, 3075–3078. https://doi.org/10.1021/bi00581a025.

Wimley, W.C., 2010. Describing the mechanism of antimicrobial peptide action with the interfacial activity model. ACS Chem. Biol. 5, 905–917. https://doi.org/10.1021/cb1001558.

Wu, Q., Patočka, J., Kuča, K., 2018. Insect antimicrobial peptides, a mini review. Toxins 10, 461. https://doi.org/10.3390/toxins10110461.

Zweytick, D., Japelj, B., Mileykovskaya, E., Zorko, M., Dowhan, W., Blondelle, S.E., Riedl, S., Jerala, R., Lohner, K., 2014. N-acylated peptides derived from human lactoferricin perturb organization of cardiolipin and phosphatidylethanolamine in cell membranes and induce defects in escherichia coli cell division. PLoS ONE 9, e90228. https://doi.org/10.1371/journal.pone.0090228.

**Supplementary Material**

a)

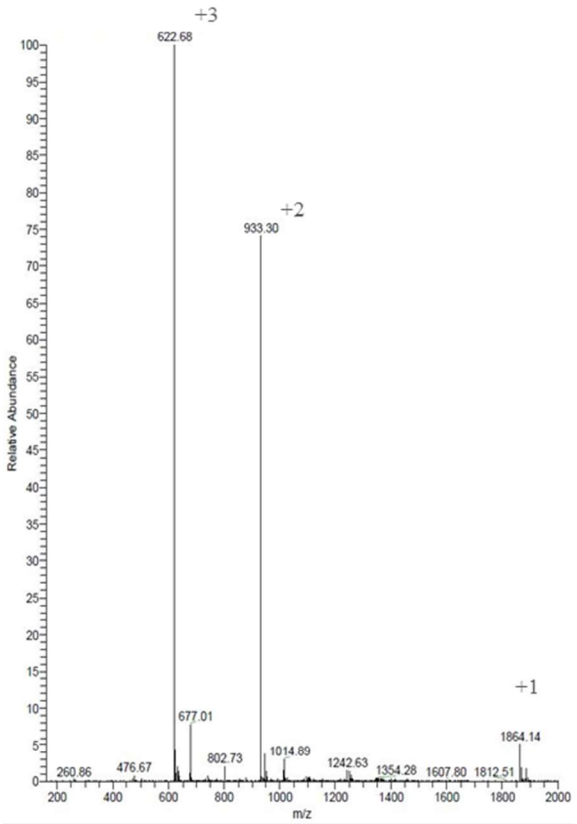


b)

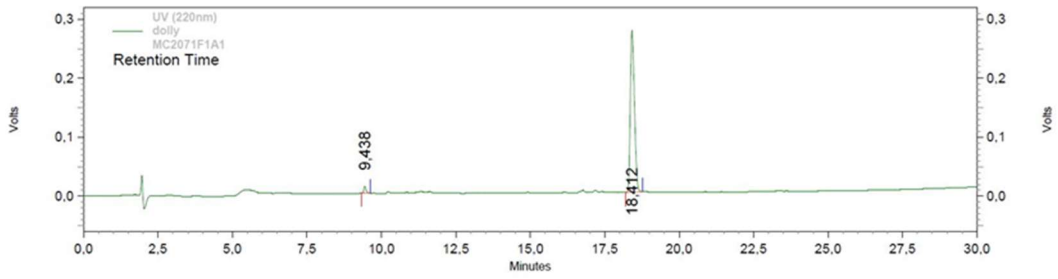


**UV (220nm)**

| Pk # | Retention Time | Area | Area % | Height | Height % |
|---|---|---|---|---|---|
| 1 | 9,438 | 58652 | 2,178 | 11484 | 4,024 |
| 2 | 18,412 | 2634408 | 97,822 | 273877 | 95,976 |
| Totals | | 2693060 | 100,000 | 285361 | 100,000 |

**Figure SM1** Hya1 mass spectrum (a). The reverse phase HPLC chromatographic profile of Hya1 (b).

a)

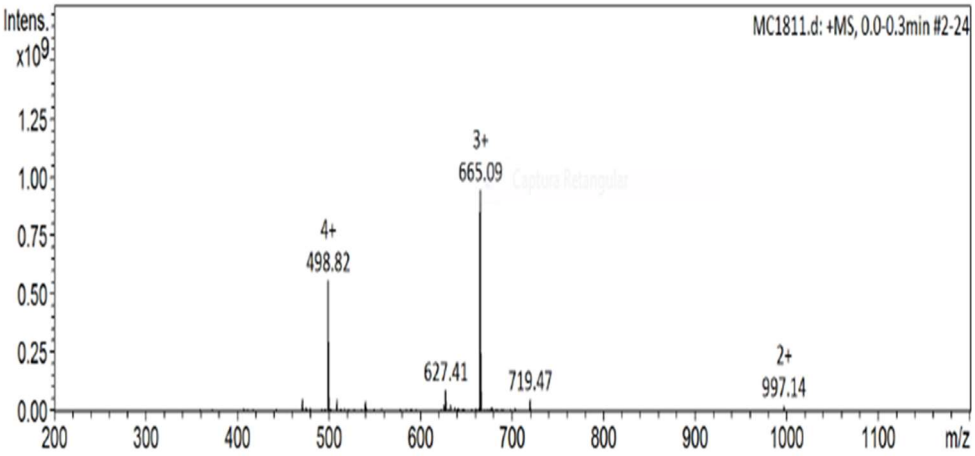


b)

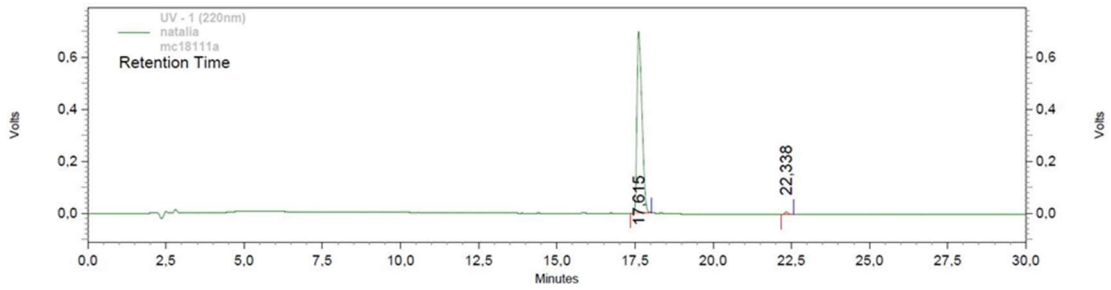


**UV - 1 (220nm)**

| Pk # | Retention Time | Area | Area % | Height | Height % |
|---|---|---|---|---|---|
| 1 | 17,615 | 7731272 | 99,069 | 694924 | 98,655 |
| 2 | 22,338 | 72669 | 0,931 | 9477 | 1,345 |
| Totals | | 7803941 | 100,000 | 704401 | 100,000 |

Figure **SM2** $K^0$Hya1 mass spectrum (a). The reverse phase HPLC chromatographic profile of $K^0$Hya1 (b).

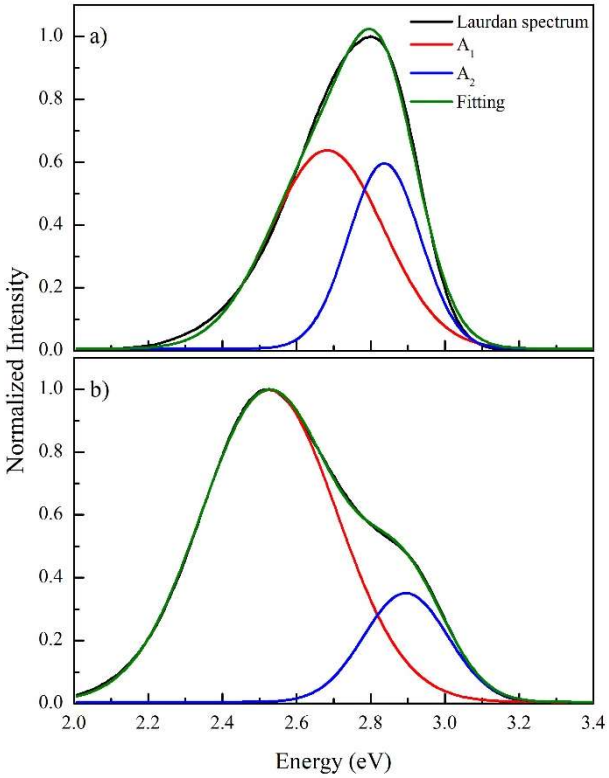


**Figure SM3** Laurdan emission spectra (black lines) in gel DPPG at 20 ºC (a) and in fluid DPPG liposomes at 50 ºC (b), together with their decomposition into two Gaussian lines: red line indicates the lower energy Gaussian band, and the blue lines the higher energy one. The fittings are shown in dark green.

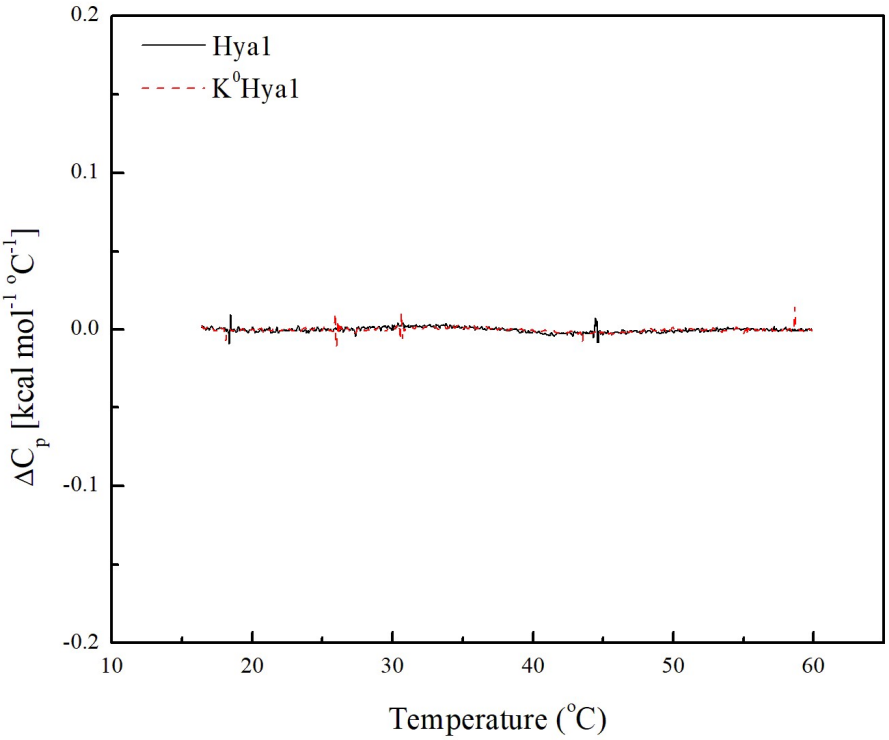


**Figure SM4** DSC thermograms of 300 µmol $L^{-1}$ Hya1 (black line) and $K^0$Hya1 (red dashed line) in buffer (Hepes 10 mmol $L^{-1}$, NaCl 3 mmol $L^{-1}$, EDTA 1 mmol $L^{-1}$, pH 7.4).

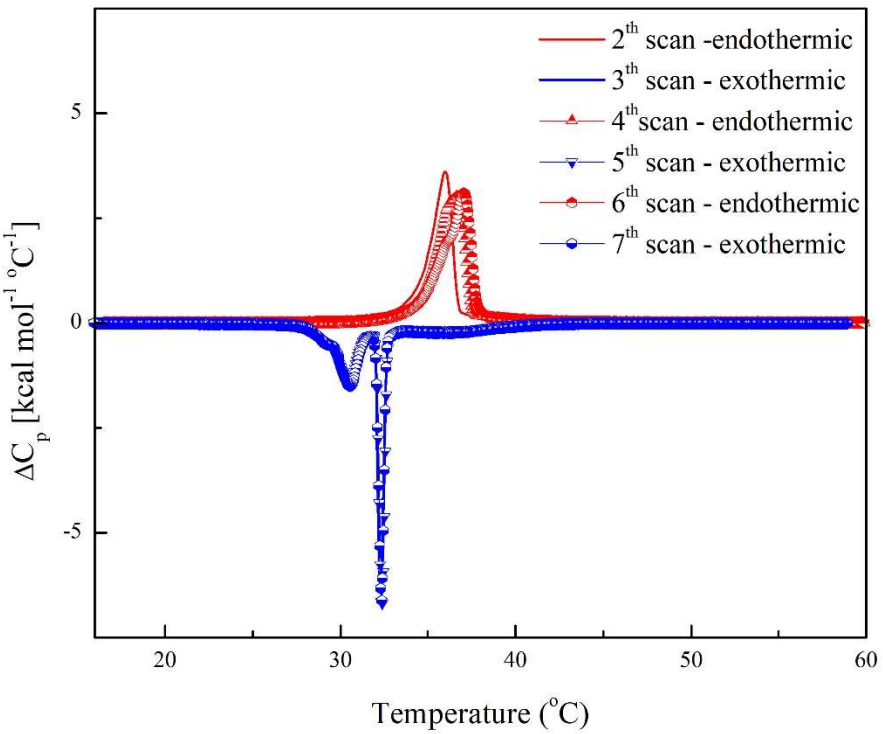


**Figure SM5** DSC thermograms of DPPG (3 mmol $L^{-1}$) in the presence of 10 mol % $K^0$Hya1 under endothermic (red lines) and exothermic (blue lines) conditions, at a sequence of different scans at a scan rate of +20 °C/h.

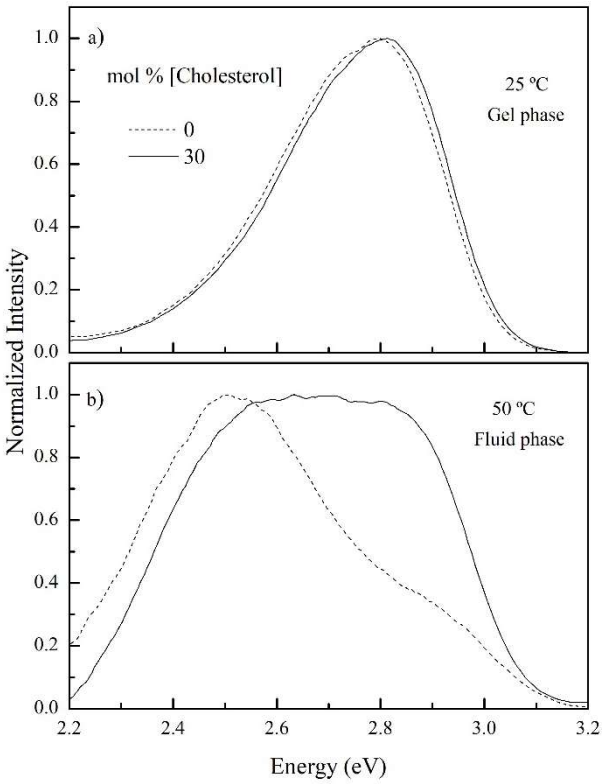


**Figure SM6** Fluorescence spectra of Laurdan incorporated into vesicles composed of pure DPPG (solid line) and DPPG with 30 mol% of cholesterol (dashed line), at the membrane gel (a) and fluid (b) phases. Excitation light beam at 340 nm.

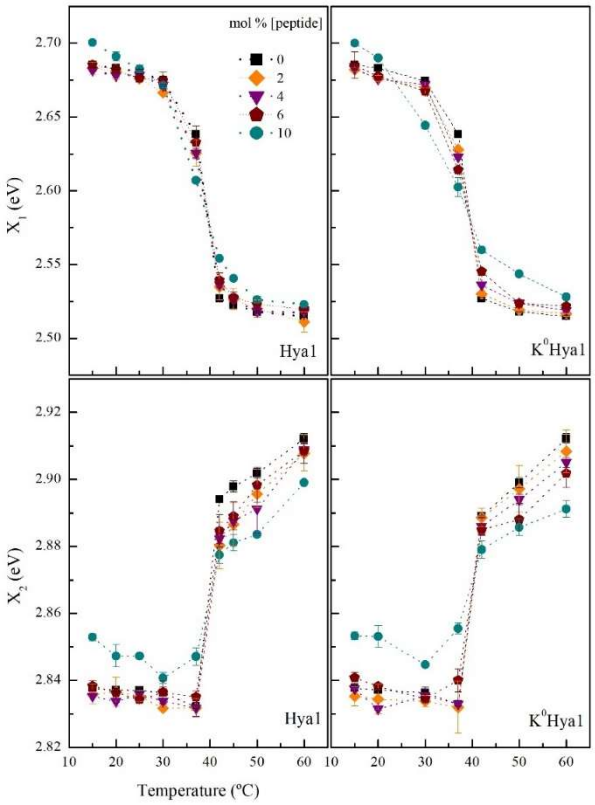


**Figure SM7** Center of the lower ($X_1$) and higher ($X_2$) energy Gaussians as a function of the temperature in the absence and with increasing peptide concentrations.

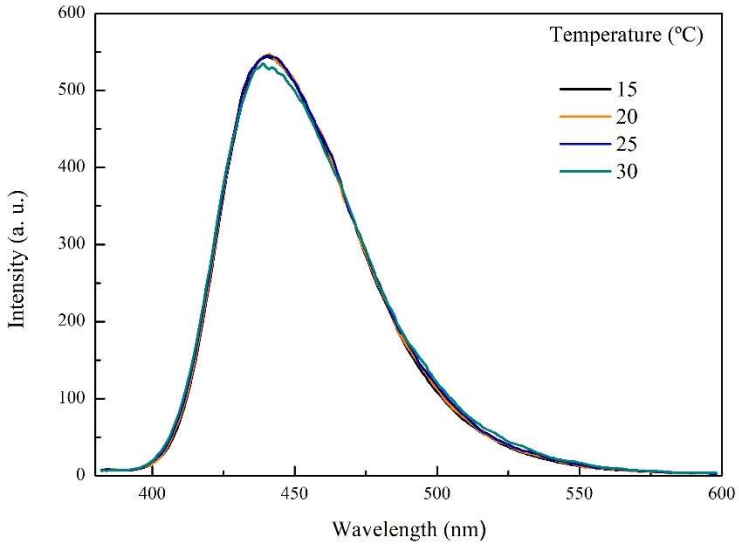


**Figure SM8** Fluorescence spectra of Laurdan (5 µmol $L^{-1}$) incorporated into gel DPPG (500 µmol $L^{-1}$) vesicles at different temperatures: 15 ºC (black line), 20 ºC (orange line), 25ºC (blue line), and 30 ºC (dark line). Excitation light beam at 340 nm.

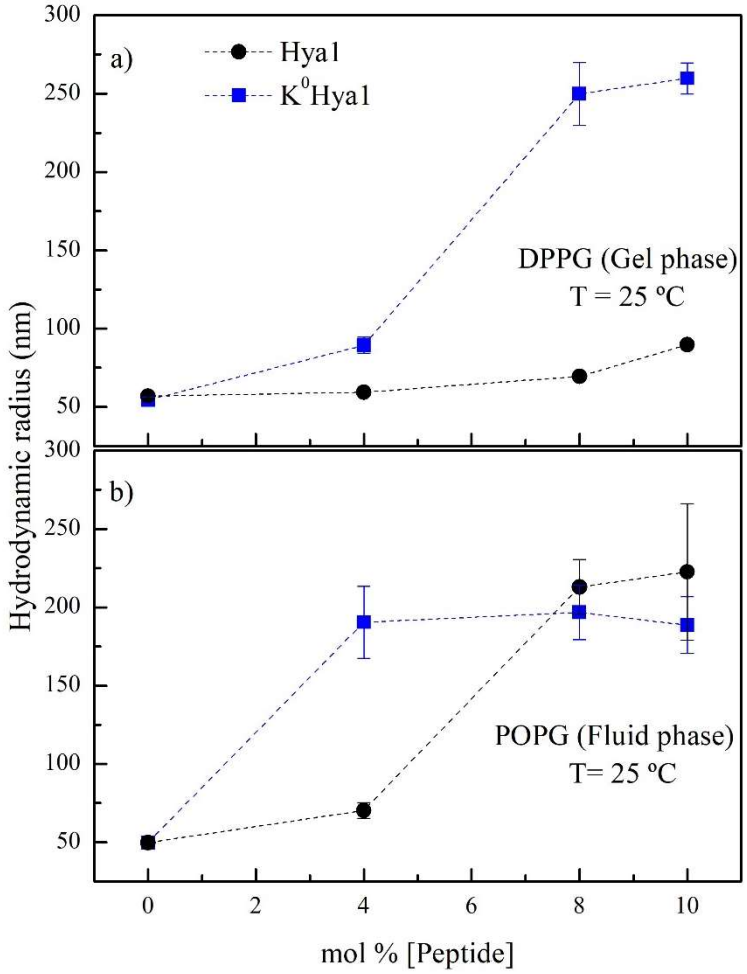


**Figure SM9** Hydrodimanic radius determined by DLS for gel DPPG (a) and fluid POPG (b) dispersions at 25 ºC, in the absence and with increasing amounts of Hya1 (black circles) and $K^0$Hya1 (blue squares).

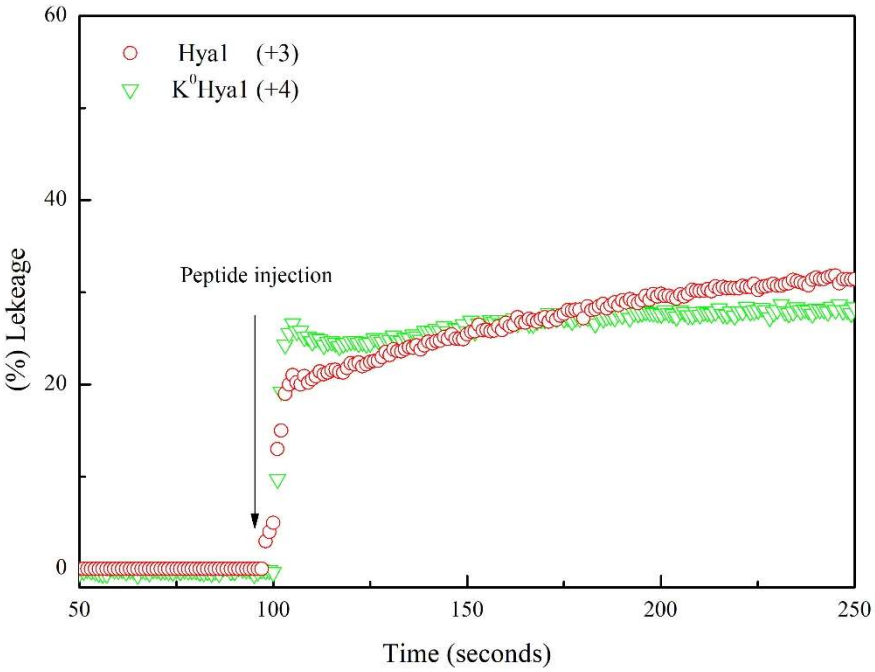


**Figure SM10** Kinetics of CF leakage through LUVs composed of gel membranes of DPPG (100 µmol $L^{-1}$) in the presence of Hya1(red circles) or $K^0$Hya1 (green down triangles). [AMP] = 8µmol $L^{-1}$). This figure is an amplification of the first 250 s of the kinetics (Fig. 10).